Active Targets and Time Projection chambers as new tools for probing EoS and clustering

T. Marchi, INFN-LNL

Outline

- PART 1 - Active Targets
  - The concept
  - Worldwide overview
  - Clustering studies with Ats
  - Probing EoS with ATs

- PART 2 – ACTAR TPC and SpecMAT as a prototypes
  - From the ACTAR Demonstrator to ACTAR TPC
  - SpecMAT
  - “Detector’s mixing”

- Outlook: the near future at LNL/LNS for the ACTAR Demonstrator

Active Target essentials

- Gas medium is both target and detection gas
- Segmented detection plane
- Drift times recorded + charge deposition on segments (works as a ***TPC***)
- Auxiliary detectors on the sides of the chamber

Advantages:

- <u>High efficiency and low detection thresholds</u>
- Wide angular coverage
- Interaction Vertex Reconstruction

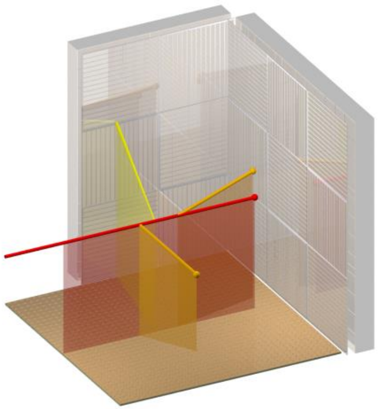

Measure many reactions AND beam energies at the same time

Active Targets around the World

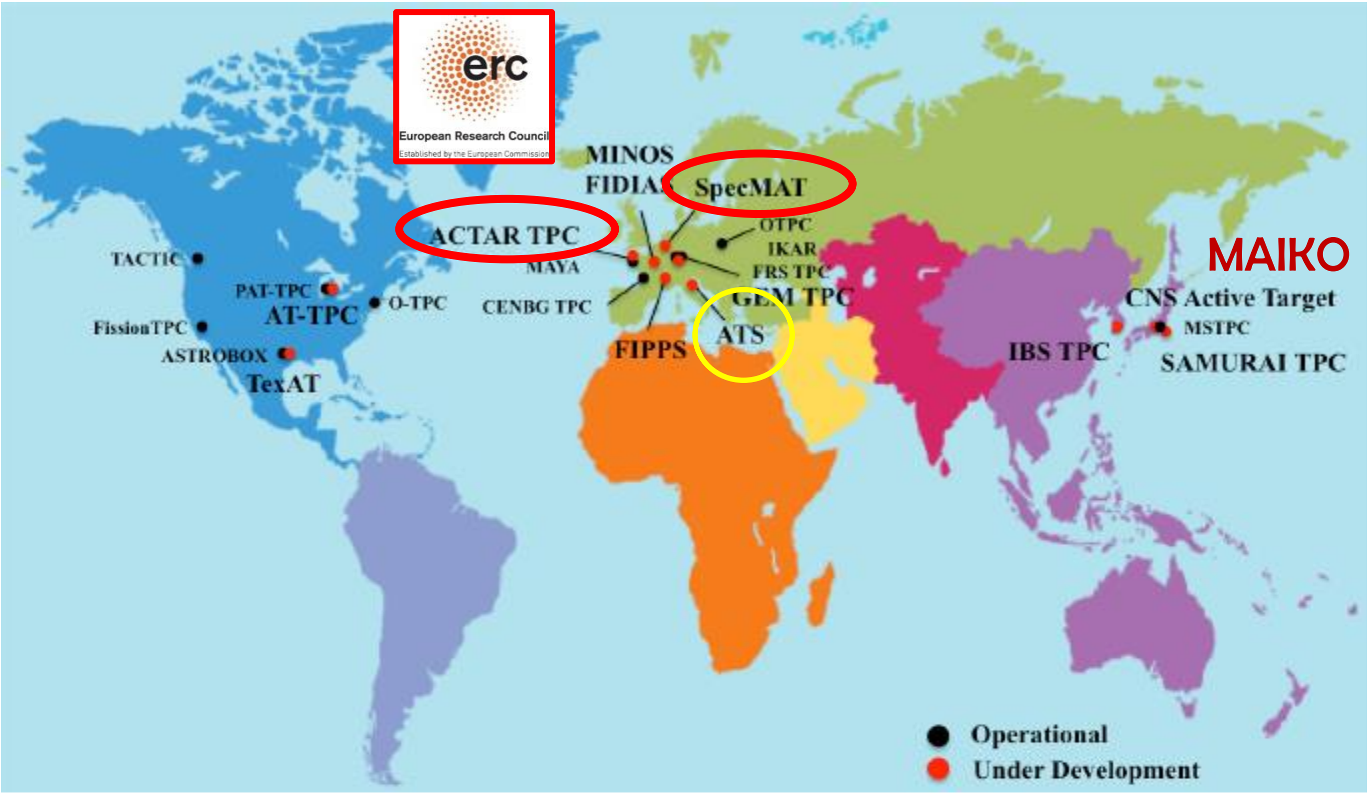

G.F. Grinyer, J. Pancin, T. Roger, EURISOL meeting 2014

Recent review about Active Target detectors:

S. Beceiro-Novo, T.Ahn, D. Bazin, W. Mittig, Prog. in Part. & Nucl. Physics (2015) 124- 165,

“Exotic” structures and clusters

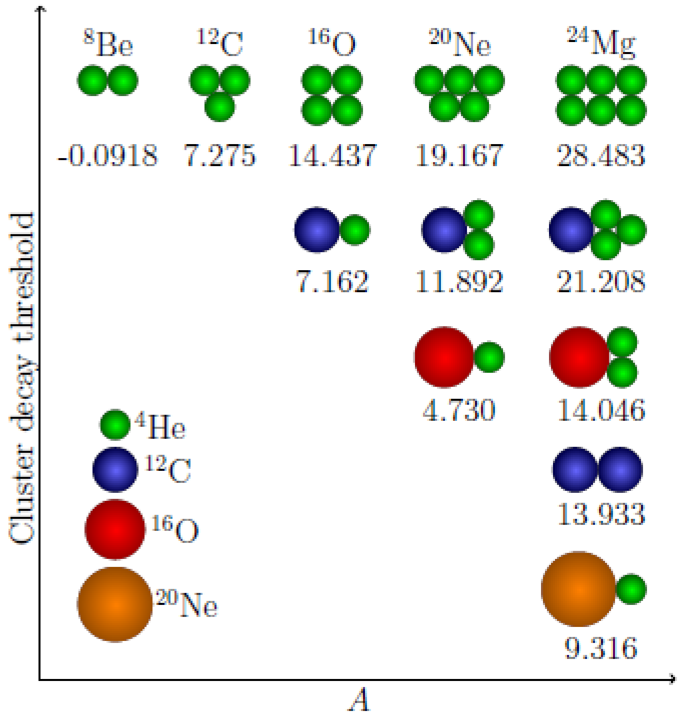

- Rotational bands in stable and unbstable nuclei
- Structure of mirror systems
- Nature of states at decay thresholds

- Non statistical decay of compound nuclei
- Direct vs Sequential Decay in HIC

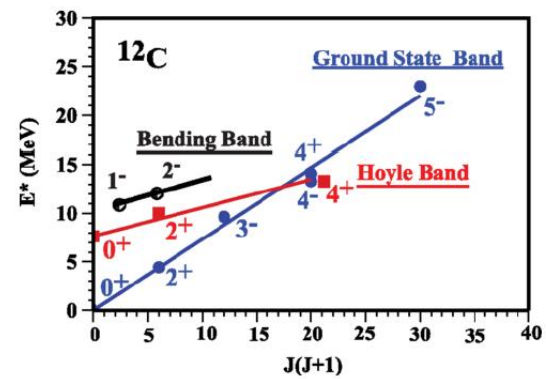

Probes:

- Resonant elastic scattering
- Transfer reactions
- Central Collisions

A. Di Pietro, I. Lombardo

IWM-EC 2018

M. Cicerchia, L. Quattrocchi

ATs and resonant elastic scattering

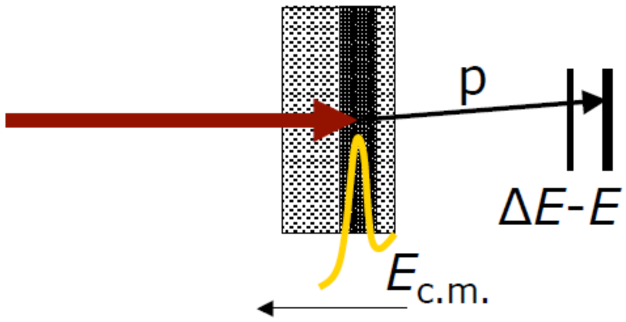

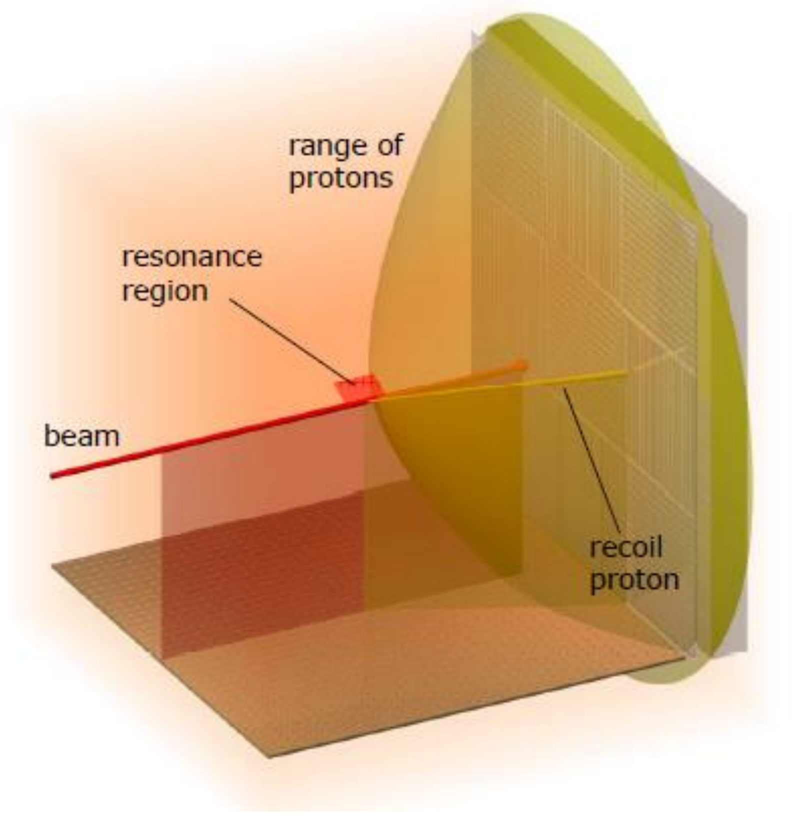

- Tracking of the interaction vertex
- Thick target
- High angular coverage
- Low thresholds
- Reaction mechanism’s tagging

Giant Resonances and Nuclear Incompressibility via Inelastic scattering

$$E_M = \sqrt{\frac{\hbar^2 K_A}{m_0^* \langle r^2 \rangle_0}} \qquad K_A = K_v + K_s A^{-1/3} + (K_{\tau v} + K_{\tau s} A^{-1/3}) \frac{(N-Z)^2}{A^2} + \dots$$

$$K_\infty = 9\rho^2 \frac{\partial^2}{\partial \rho^2} \left[\frac{E(\rho)}{A} \right]_{\rho=\rho_0} \qquad K_A = 0.64 K_\infty - 3.5\ MeV$$

$$K_\infty = 225 - 240\ MeV$$

- The centroid of the ISGMR is linked to the compression modulus of the Nucleus (K_a)
- From K_a, the nuclear incompressibility can be inferred
- Studies of K_a as a funcion of isospin are needed
- Inelastic scattering of (un)stable nuclei on alpha and deuteron are good probes for ISGMR.

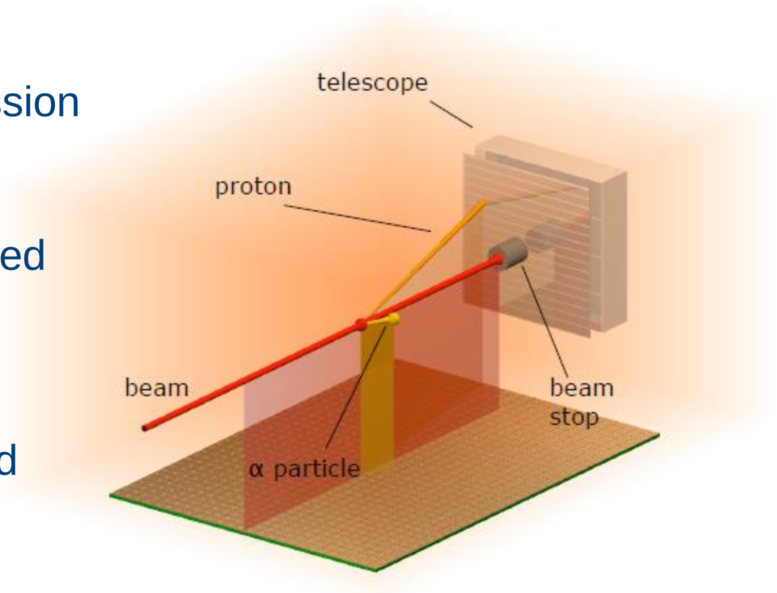

Study of the ISGMR and in ISGQR using inelastic scattering

$^{68}Ni(\alpha,\alpha')^{68}Ni^*$

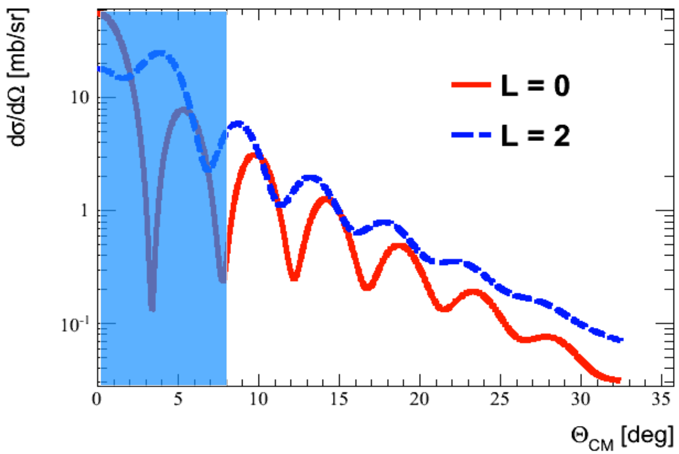

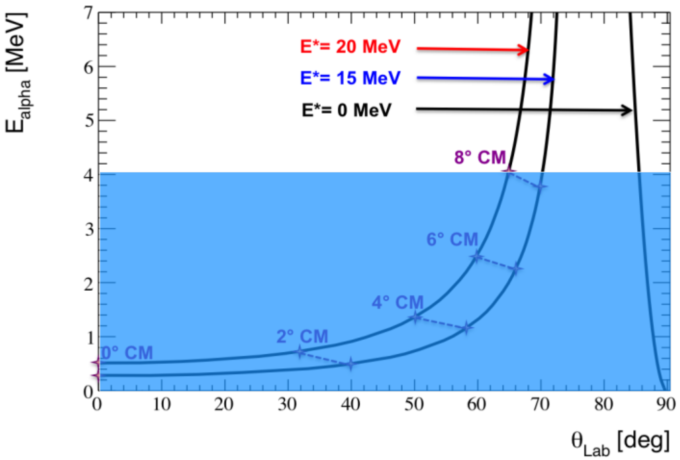

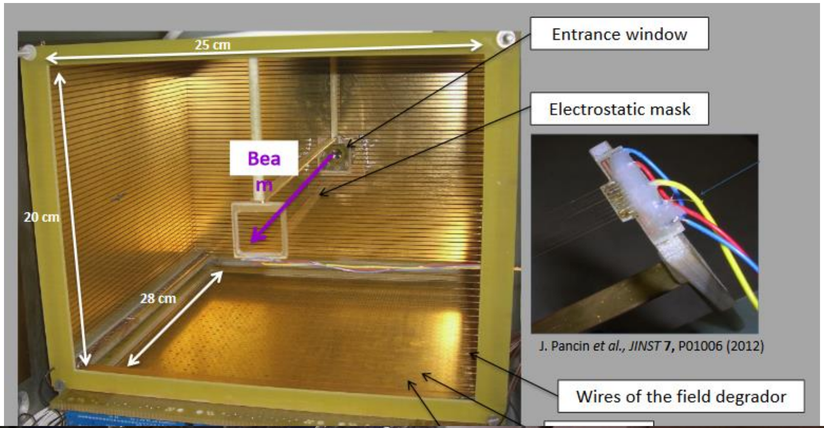

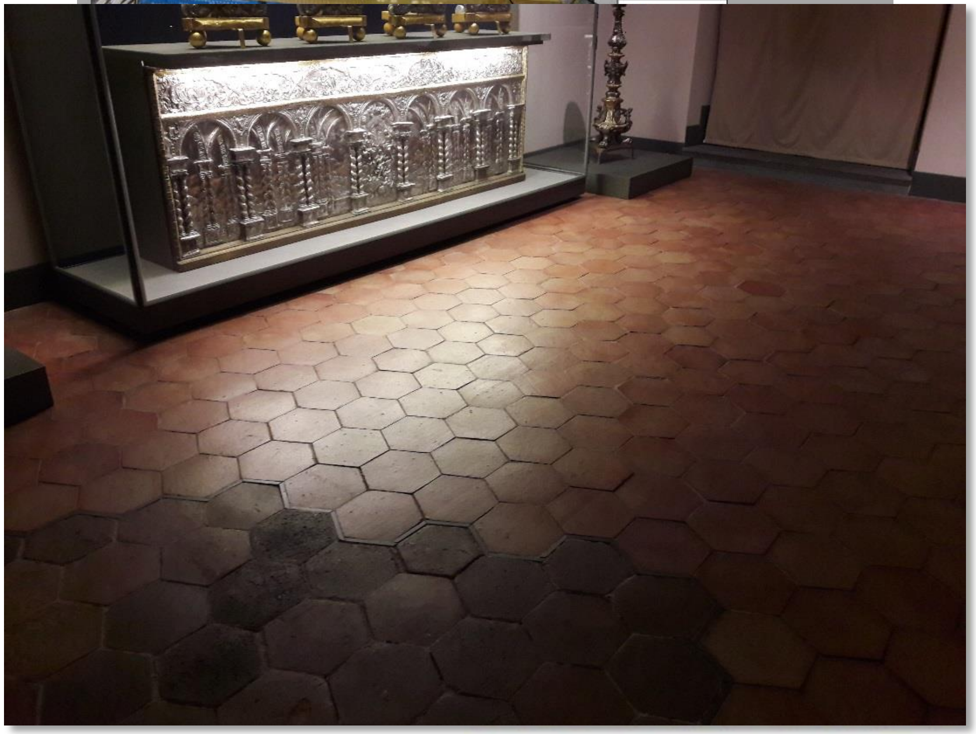

Study of the ISGMR and in ISGQR using inelastic scattering

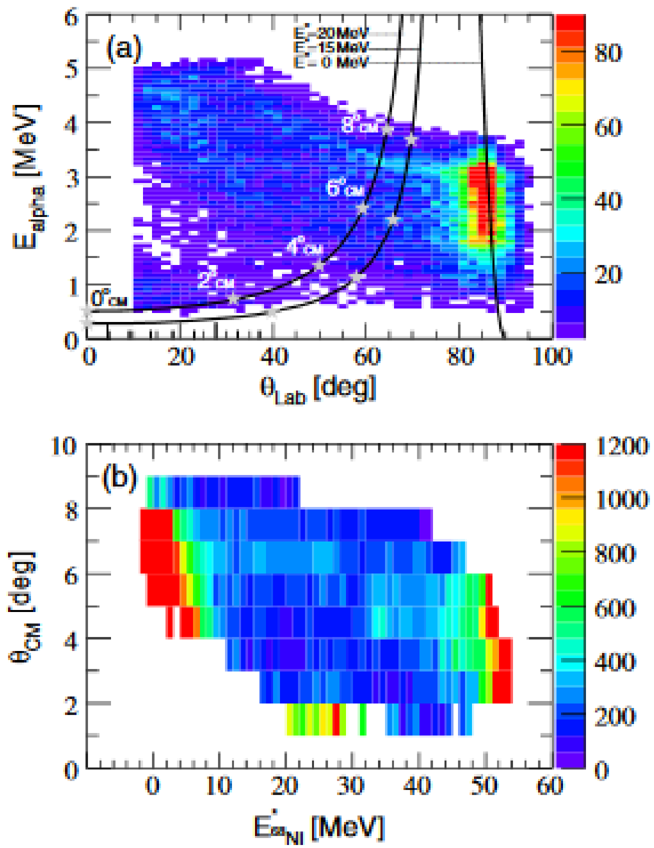

FIG. 1 (color online). (a) Scatter plot of recoiling alpha energy versus scattering angle in the laboratory frame for the ^{68}Ni beam. (b) Corresponding events transformed in the c.m. frame, and corrected for the geometrical and reconstruction efficiencies.

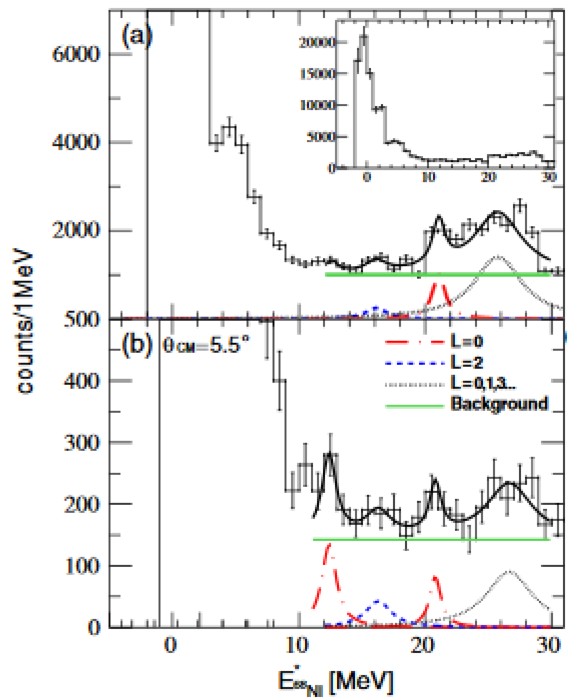

FIG. 2 (color online). (a) ^{68}Ni excitation-energy spectrum for all angles deduced from the alpha recoil kinematics and corrected for geometrical and reconstruction efficiencies. (b) Same for $\theta_{c.m.} = 5.5°$. For both spectra, the subtracted background is indicated by the horizontal green solid line. The data were fit with Lorentzians at 12.9 MeV (red dot-dashed line), 15.9 MeV (blue short-dashed line) and 21.1 MeV (red dot-dashed line) for the low-energy mode, the isoscalar giant quadrupole resonance (ISGQR) and the ISGMR, respectively (see text). Statistical uncertainty and the estimated uncertainty on the efficiency correction are taken into account.

M. Vandebrouck et al., PRL 113, 032504 (2014)

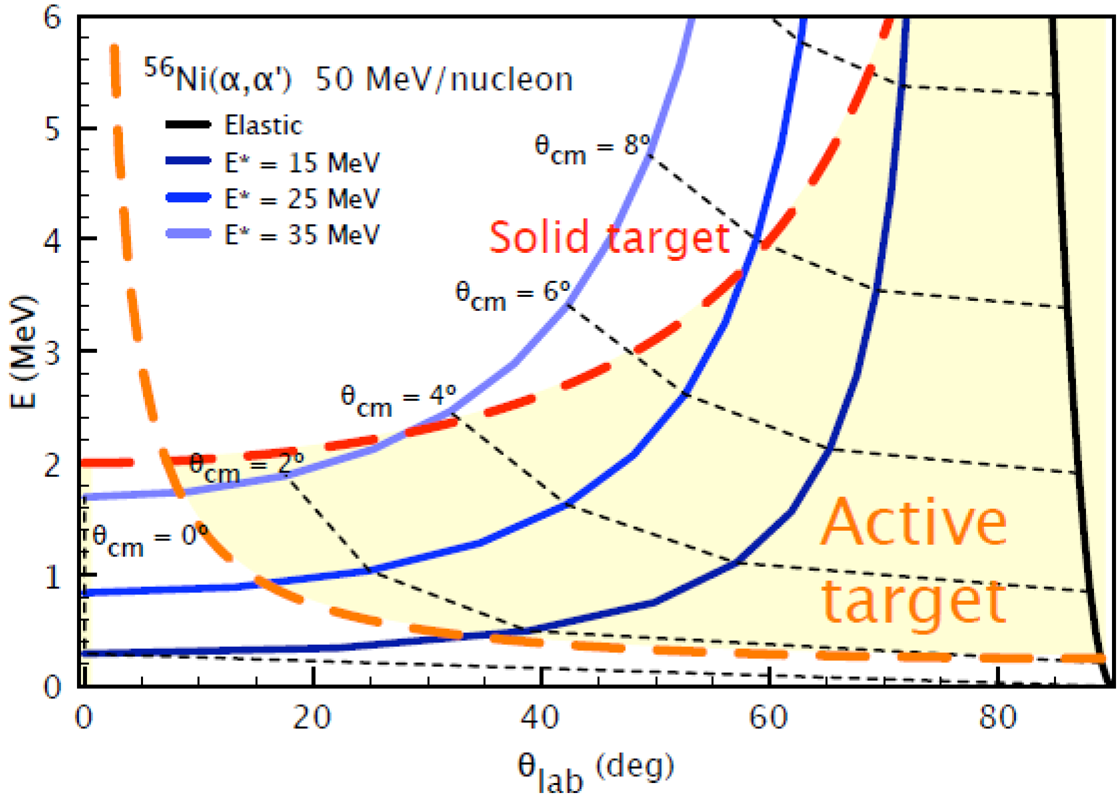

Figure 16: Kinematic plot for ^{56}Ni(α,α') inelastic scattering at various excitation energies in ^{56}Ni. The dashed curves represent the limits of detection by using a conventional foil target (in red) and a gaseous active target (orange) calculated from the ranges of the α particles. The yellow-painted area is only accessible by the active target.

When the issues are neither the beam intensity nor the energy loss in the target…

Heavy Ion Collision to study the density dependent symmetry energy. The SPiRIT TPC at SAMURAI - RIKEN

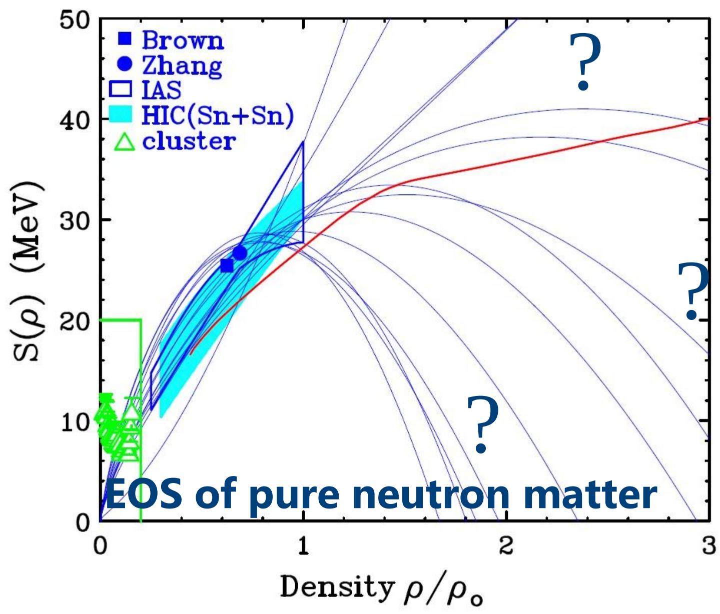

- Large uncertainty on nuclear symmetry energy at $\rho \gg \rho_0$ compared with that for $\rho \leqq \rho_0$ region.
- Heavy ion collision is currently unique way to produce high dense matter in the laboratory.
- New experimental project at RIBF for the study of density dependent symmetry energy. **$\rho \sim 2\rho_0$** nuclear matter at RIBF energy HIC.

Betty Tsang et al at GDS workshop 2018, Santiago De Compostela
Tadaaki Isobe et al at GDS workshop 2018, Santiago De Compostela

The SPiRIT TPC has a lot in common with state of the art Active targets

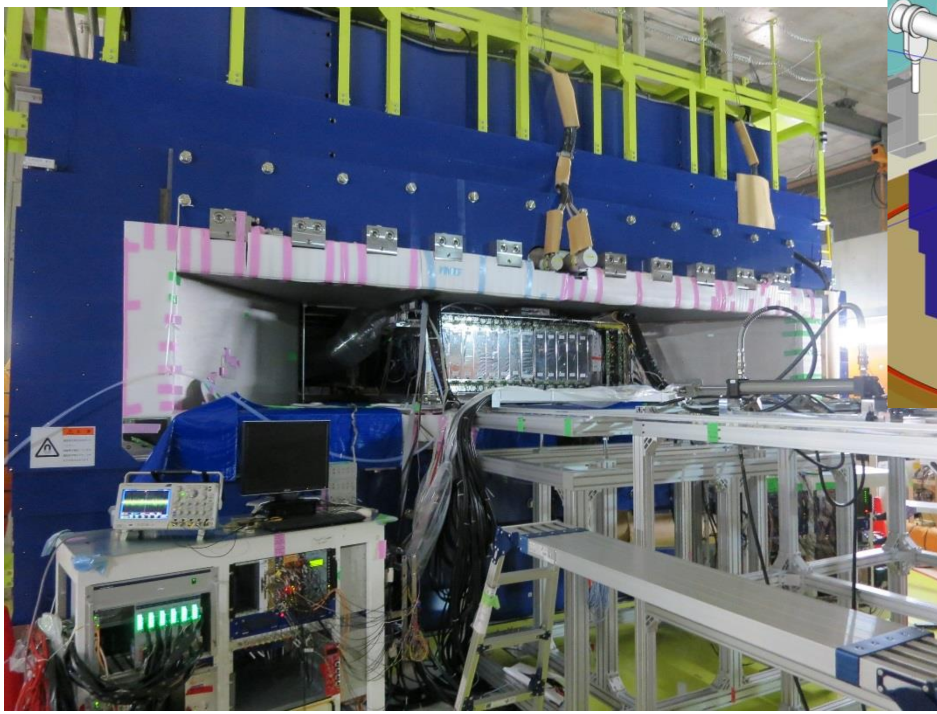

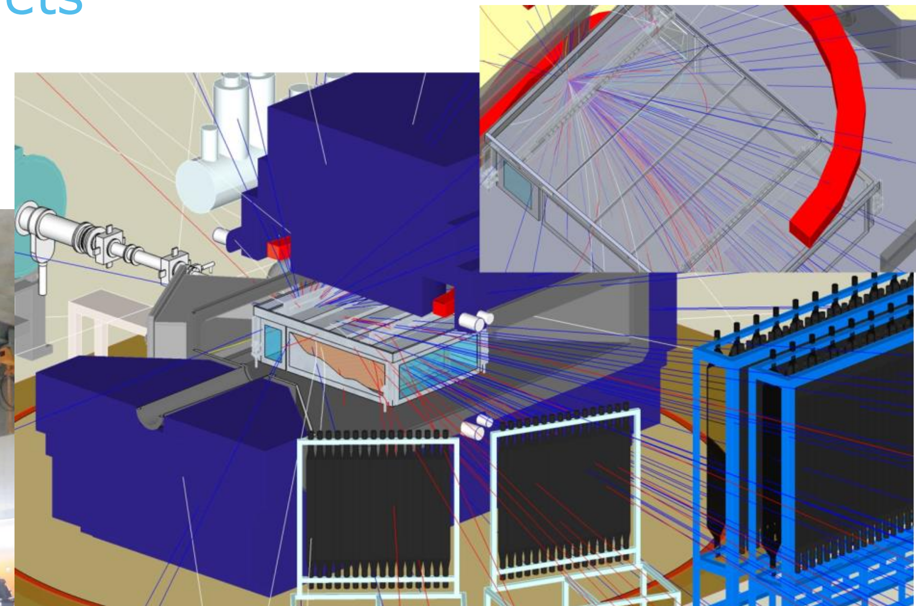

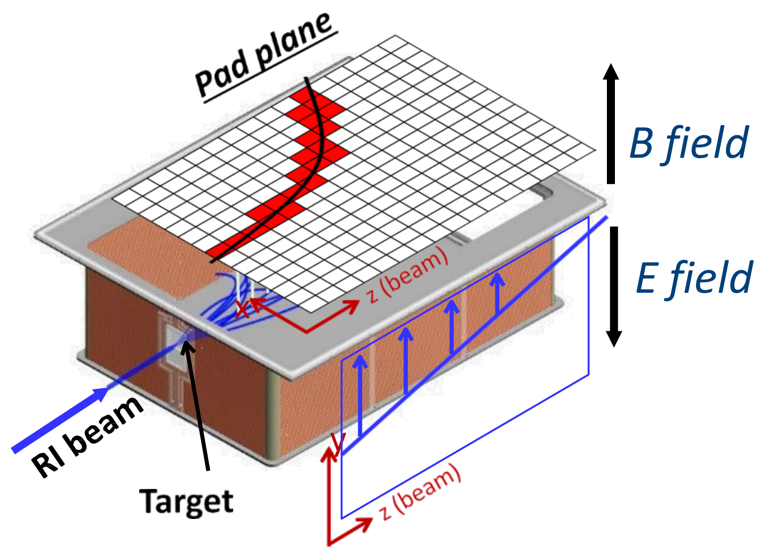

Betty Tsang et al at GDS workshop 2018, Santiago De Compostela
Tadaaki Isobe et al at GDS workshop 2018, Santiago De Compostela

SPiRIT TPC – type of events

- Reaction on target:
  good event
- Reaction upstream:
  before target
- reaction with gas inside TPC:
  Active target events;

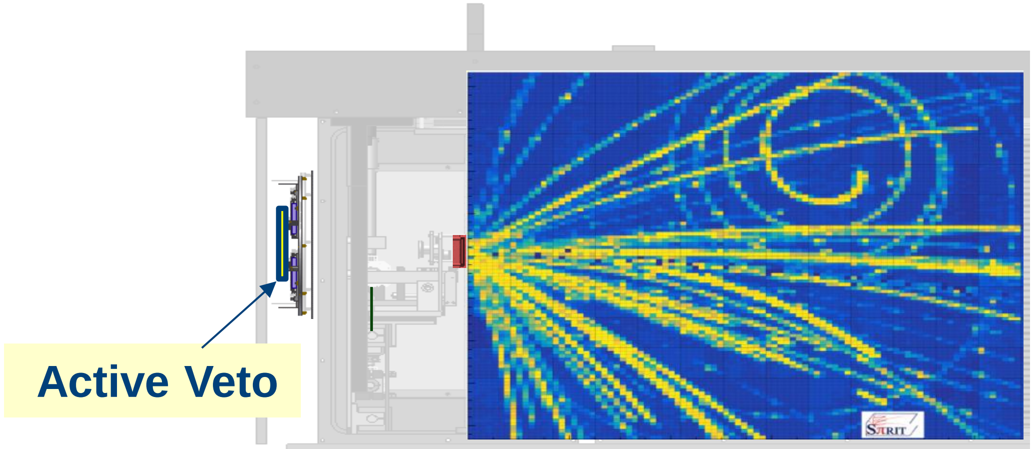

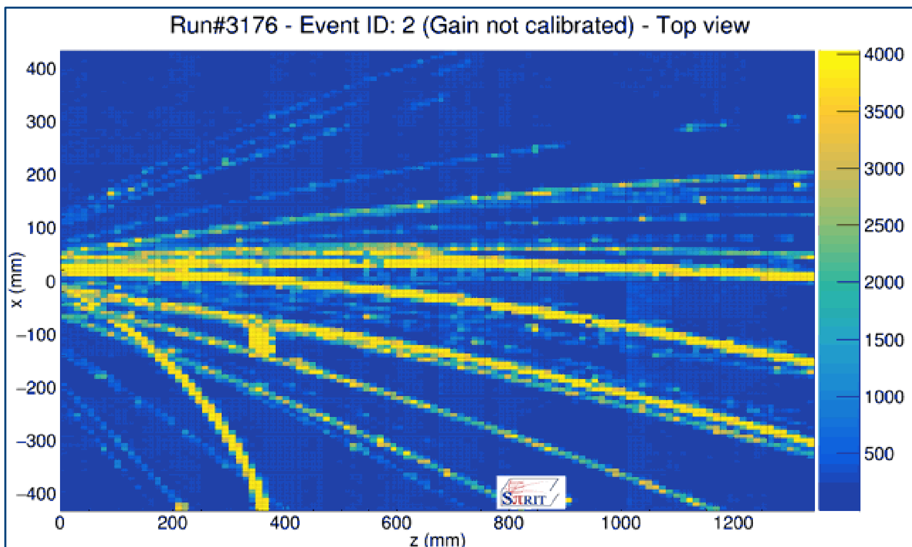

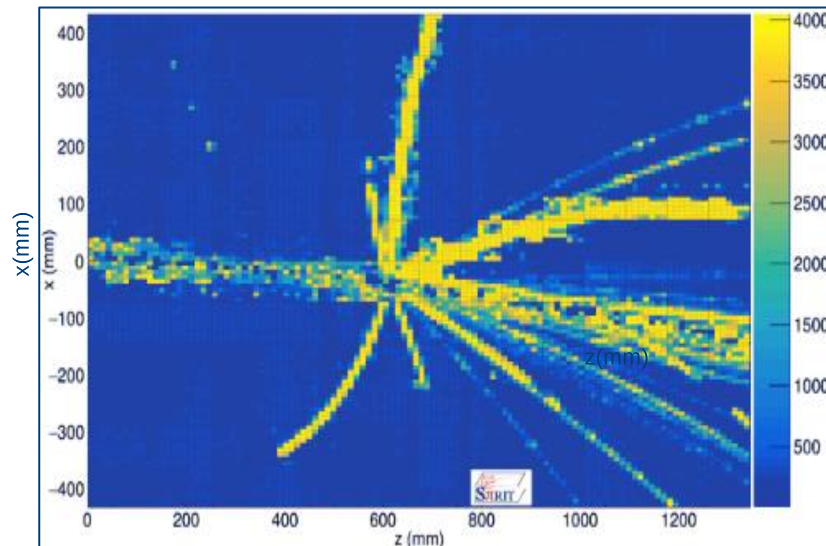

High channel numbers

- 2048 - ACTAR TPC Demonstrator, based at GANIL, Caen
- 10 024 – ATTPC Detector at NSCL, Michigan
- 12096 – SPiRIT TPC, RIKEN
- ~10k – SpecMAT, KU Leuven
- 16 284 – ACTAR TPC final Detector

Point-to-point connections could lead to unpleasantness.

Concept electronics – ACTAR TPC
All 16284 ch. fit in these 2 racks

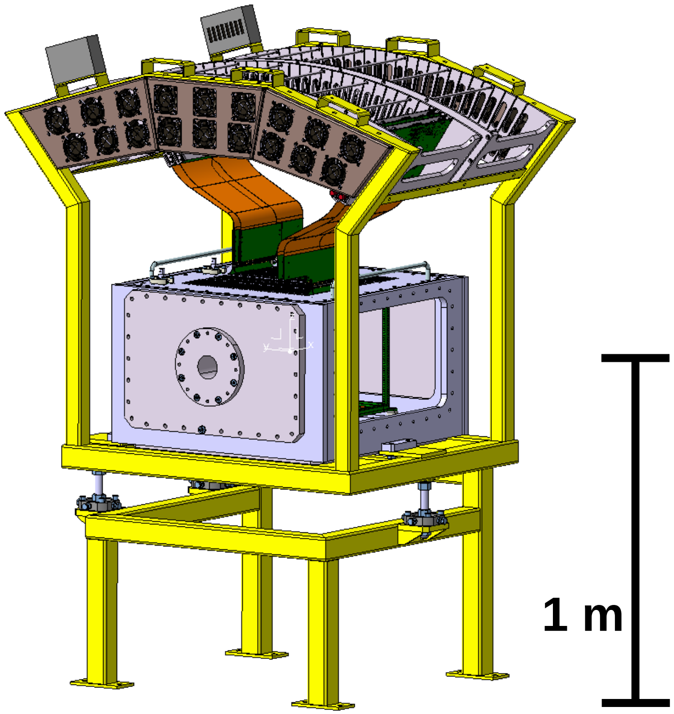

Work of P. Gangnant

- PART 2 – ACTAR TPC and SpecMAT as a prototypes
  - From the ACTAR Demonstrator to ACTAR TPC
  - SpecMAT
  - “Detector’s mixing”

Active Target and TPC – ACTAR TPC

European Research Council
Established by the European Commission

Parameter	Value	Depends upon
Dynamic range	10^3	- amplification technology - detector geometry - electronics - auxiliary detectors
Number of tracks	all tracks detected independently	- segmentation using pads - electronics
Spatial resolution	< 2 mm	- amplification technology - pad size and shape - number of channels - auxiliary detectors
Maximum beam intensity	10^6 pps	- drift velocity - operating conditions (gas type or mixture) - detector size - electronics
Timing resolution	20 ns	- drift velocity - electronics
Energy resolution (signal amplitude)	2%	- spatial resolution - operating conditions - amplification technology
Efficiency	$> 90\%$	- dynamic range - detector geometry - type of event
Counting rate for accepted events	1 kHz	- electronics - pad-to-electronics topology
Minimum half life decay events	$\approx 10\ \mu$s	- electronics
Portability		- detector design - electronics

[ACTAR TPC CDR]

- **Physics programs:**
  - **One and two nucleon transfer reactions**
  - **Rare and exotic nuclear decay (2p, β2p, …)**
  - **Inelastic scattering and giant resonances**
  - **Resonant scattering and astrophysics**
  - **Transfer-induced fission, … and more!**

ACTAR TPC: Design

European Research Council
Established by the European Commission

- **Drift Region**
  - **Electric field uniformity**
  - **2 geometries (square ~ 25x25 cm vs rectangular 12.25x25 cm)**

- **Amplification Region**
  - **MICROMEGAS*, GEM amplifiers**
  - **Fast timing, robust, cost effective**

- **Segmented pad plane**
  - **Very high-density: 2x2 mm^2 (= 25 channels/cm^2)**
  - **Total of 16384 electronics channels (GET system)**
  - **Fully digitized waveforms and times for every pad**

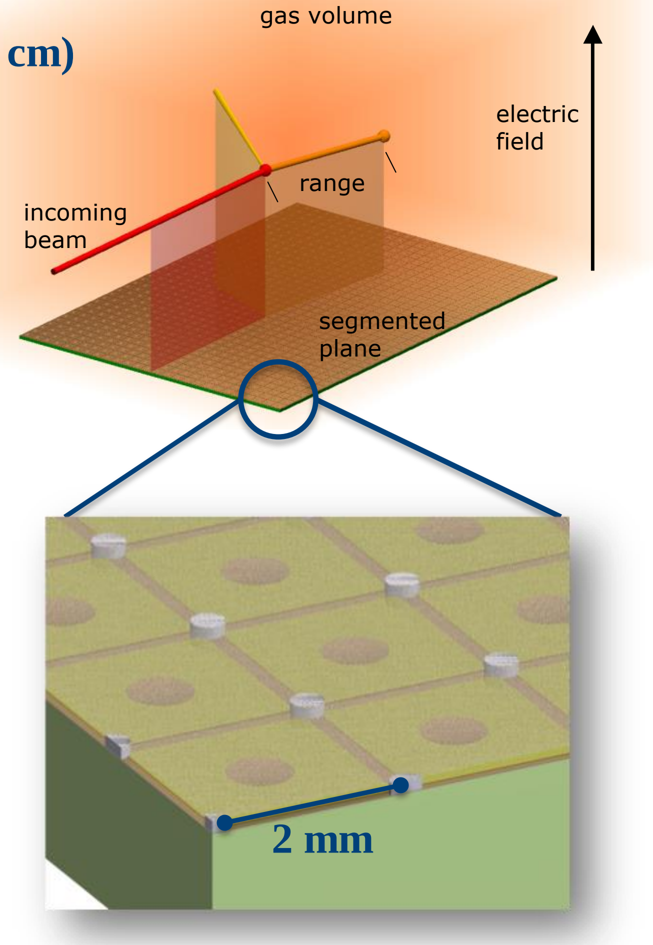

- **Design Objective: versatility**
  - **Telescopes for escaping particles (Si+Si or Si+CsI)**
  - **LaBr3 or HPGe for γ rays**

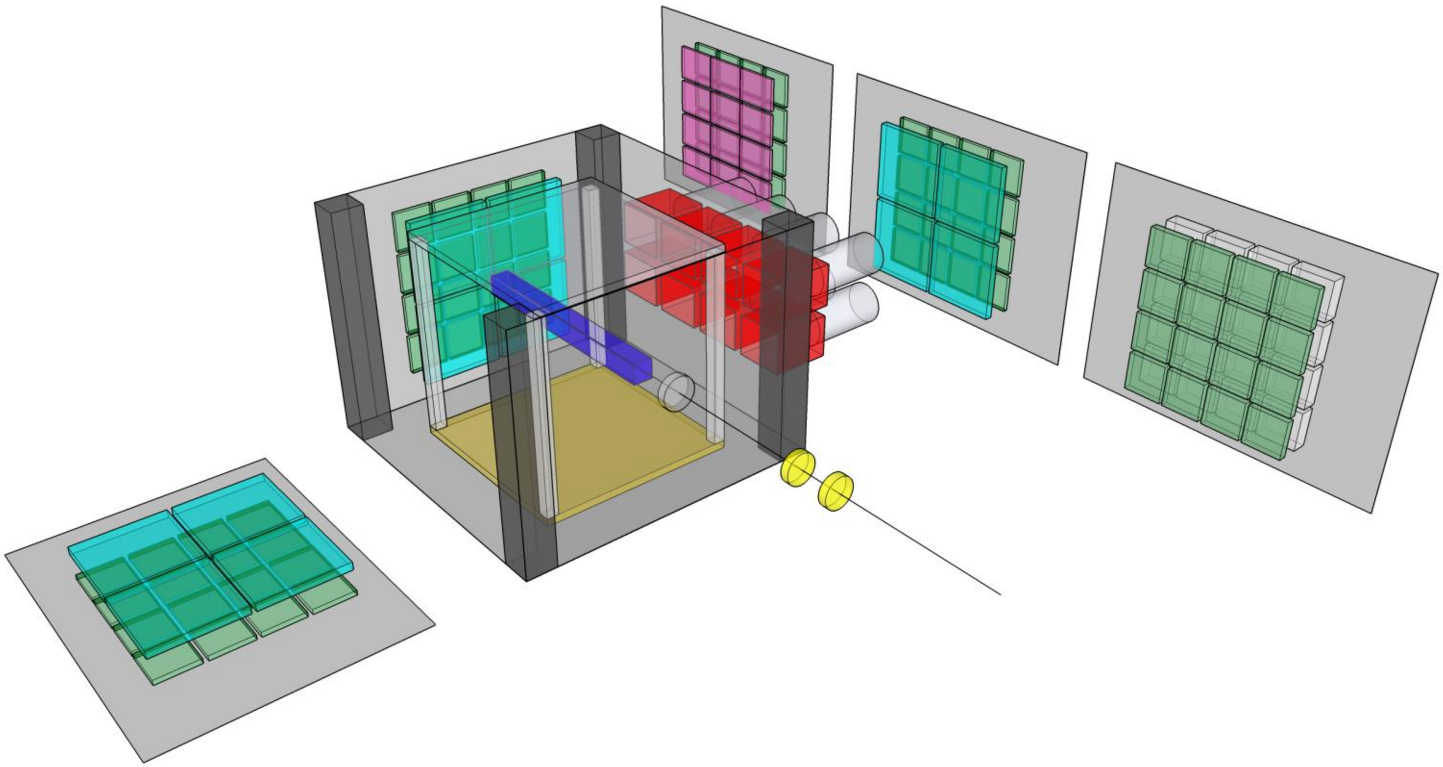

ACTAR TPC Demonstrator

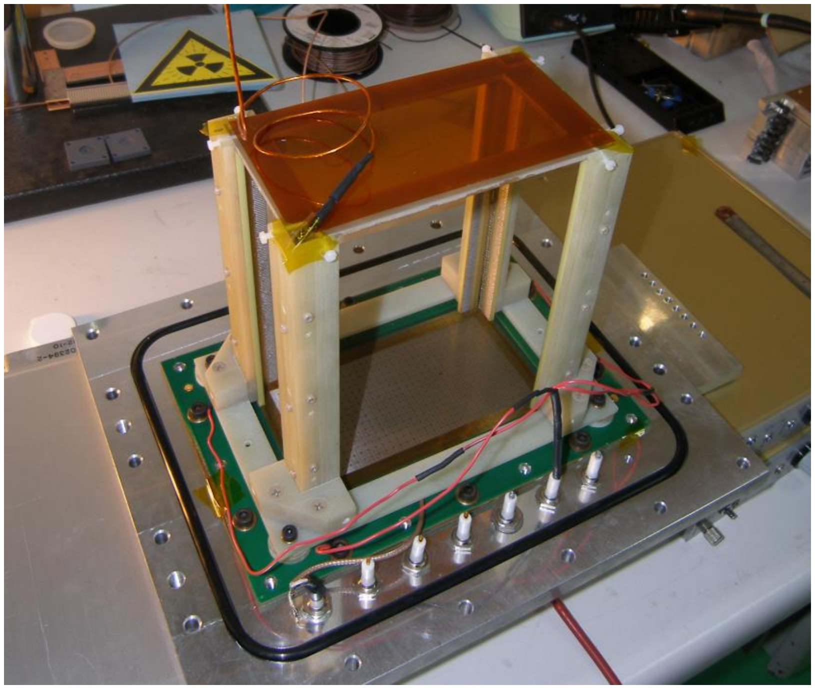

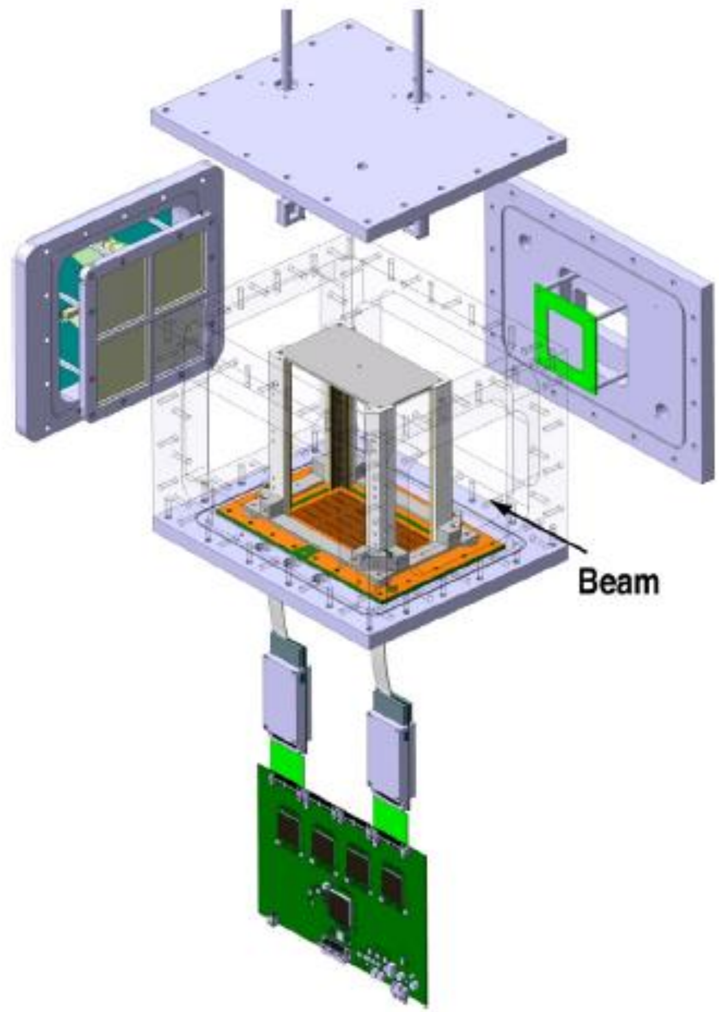

ACTAR TPC Demonstrator chamber

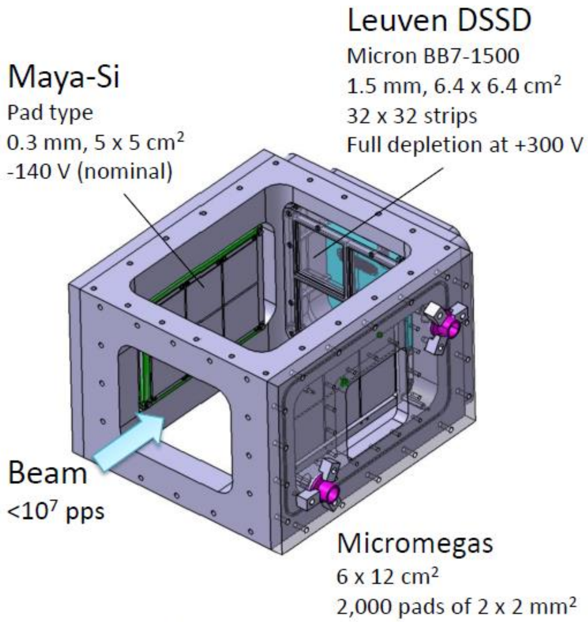

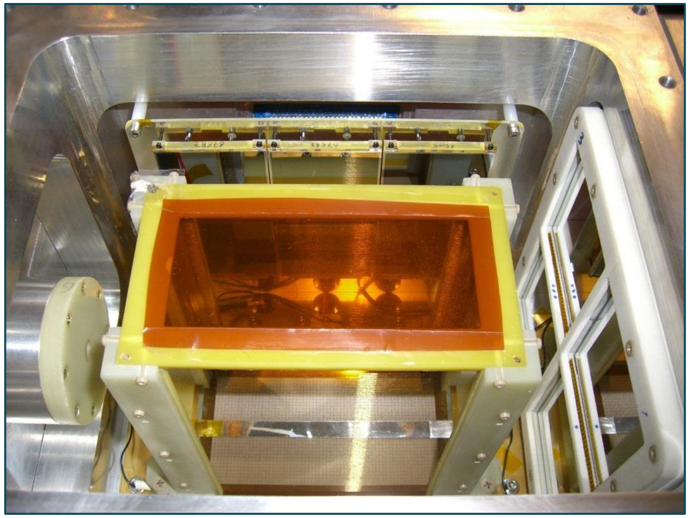

Demonstrator runs with Bacchus Spectrometer at IPN Orsay, June/July 2015

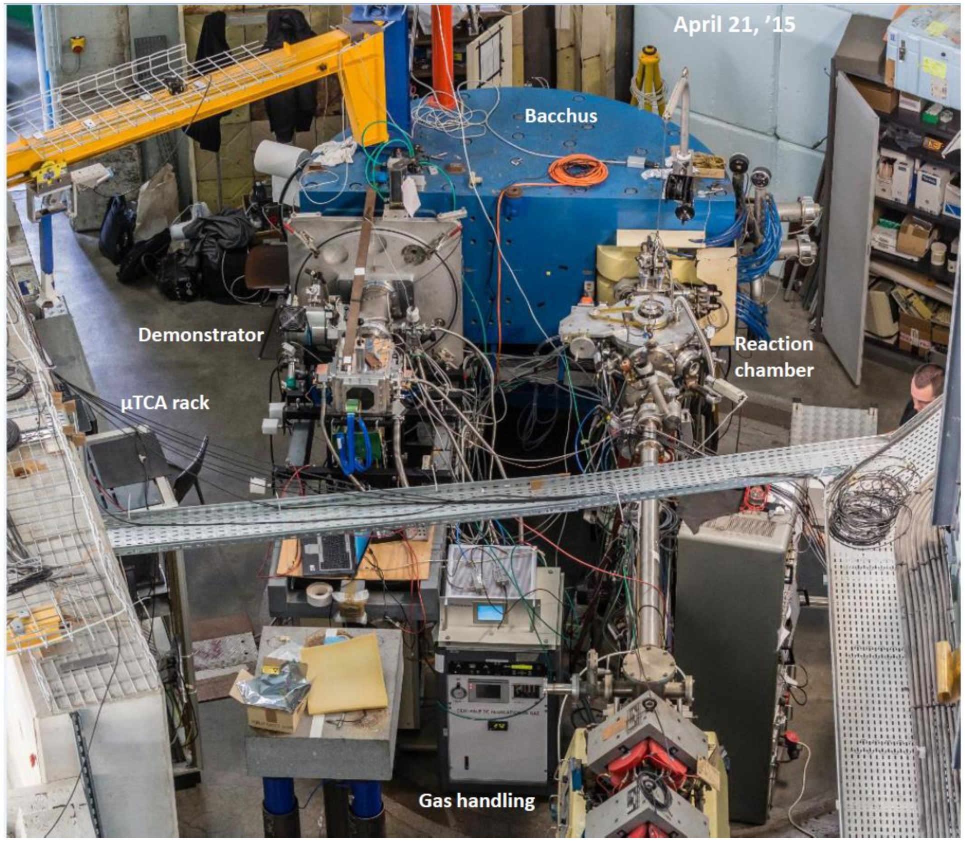

Figure and photos from D. Suzuki

ACTAR TPC Demonstrator @ IPN Orsay

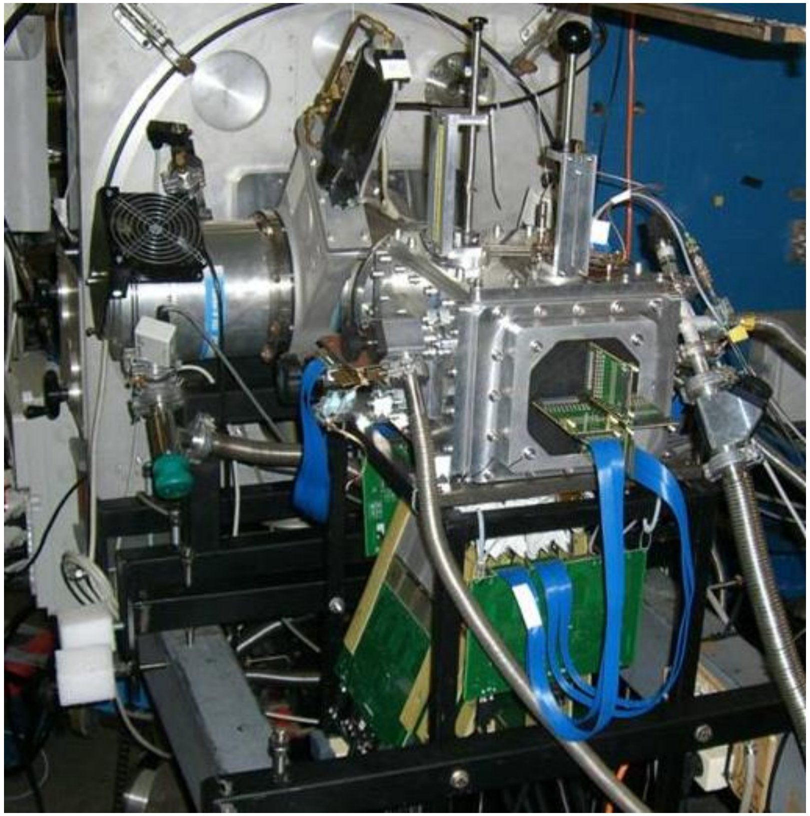

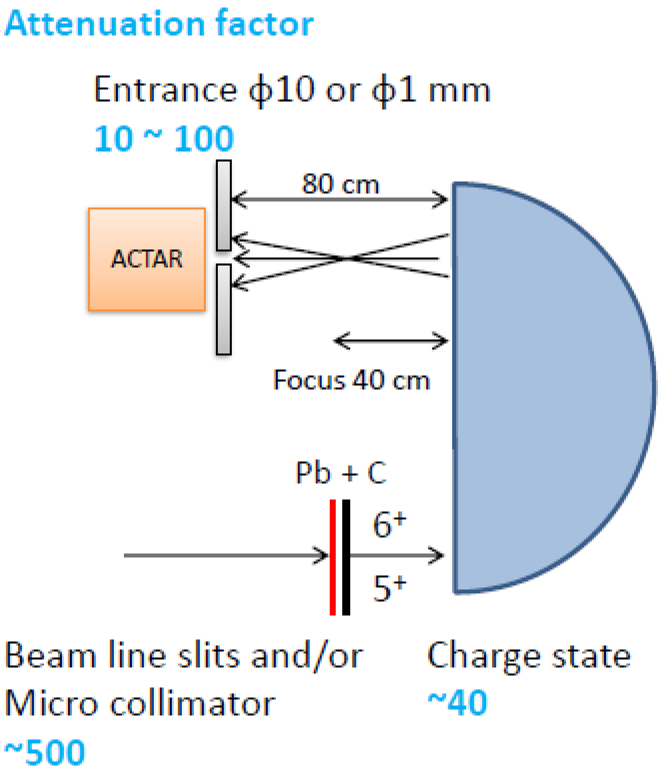

Figure and photos from D. Suzuki

IPNO 2015 : Goals

- **Physics : α clustering in light nuclei (D.Suzuki)**
  - Excitation of Hoyle states in ^{12}C
    - ^{12}C beam : inelastic scattering ($^{12}C+\alpha$)
  - Structure of excited states in ^{10}B
    - ^{6}Li beam : resonant alpha scattering ($^{6}Li+\alpha$)

Kanada-En'yo, Y. et al, PRC 91, 054323 (5 2015).

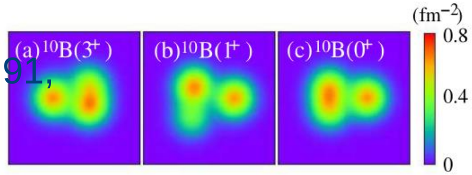

- **Detector : Ideal performance test**
  - Elastic scattering and transfer channels well known
  - Particle ID/resolution: protons to ^{12}C
  - Many-body final states – identify all 4 α particles?

- **Electronics : A relatively complex setup**
  - 256 strips DSSD (0°) + 12 Si detectors (sides)
    - Trigger with multiplicity = 1 (in GET)
  - 2048 channels for the pads (triggered by the Si)

Analysis
2 Master Thesis (KU Leuven)
1 PhD (GANIL)

Provided and are providing several input for the final design and for the validation of ACTARSim code (GEANT4 simulation)

ACTAR TPC @ IPNO

^{12}C on He:C_4H_{10}

- **2-particle event**

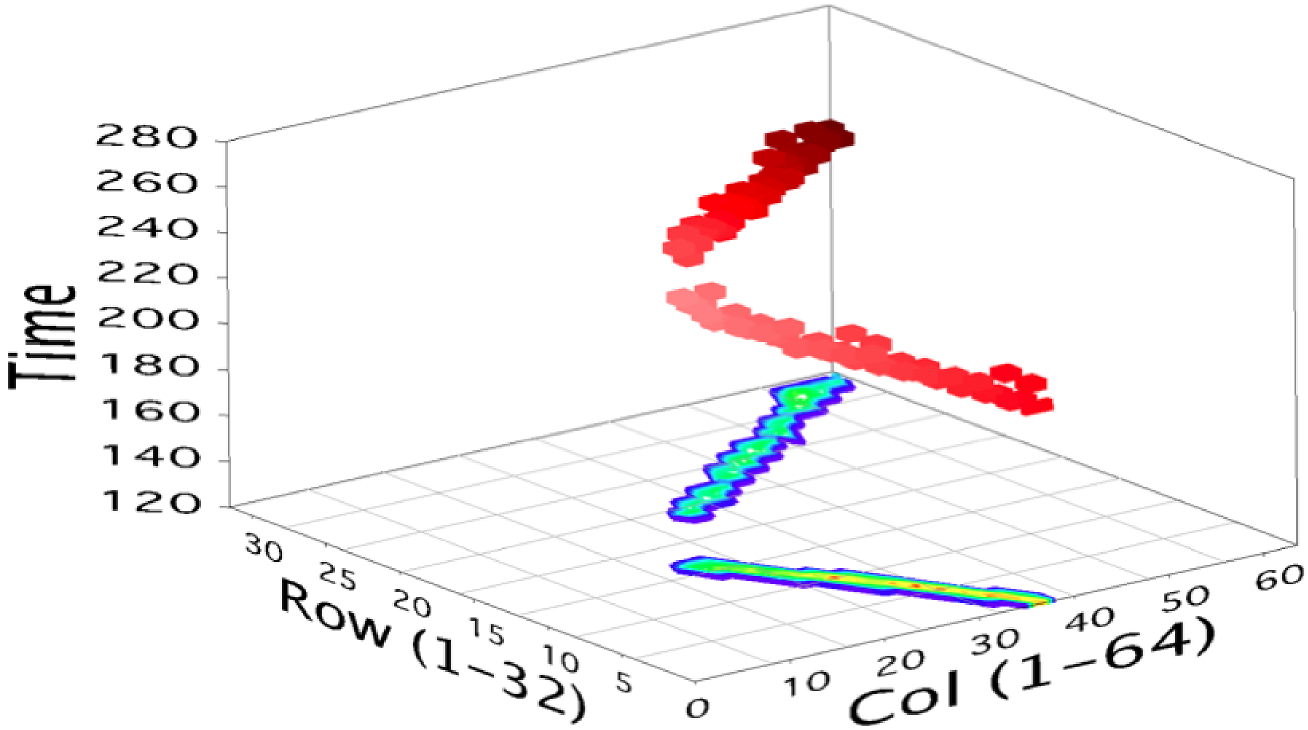

Courtesy of G.F. Grinyer

ACTAR TPC @ IPNO

^{12}C on He:C_4H_{10}

- **4-particle event**

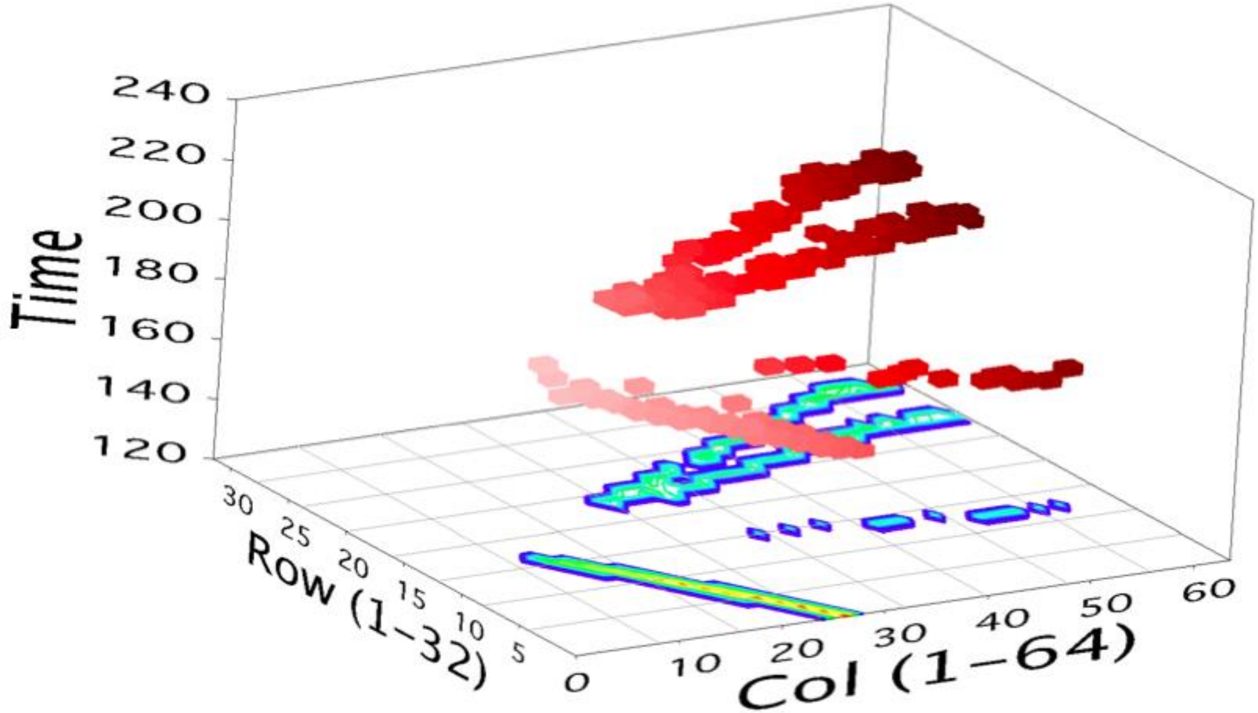

Courtesy of G.F. Grinyer

ACTAR TPC @ IPNO

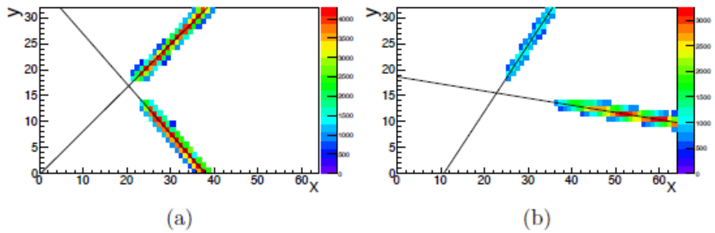

Figure 4.19: *Charge deposition on the pad plane of (a) a* $^{12}C(^{12}C,^{12}C)^{12}C$ *and (b) a* $^{12}C(\alpha,\alpha)^{12}C$ *scattering reaction.*

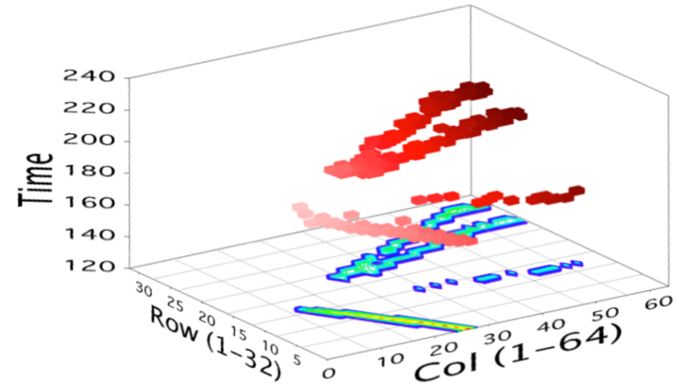

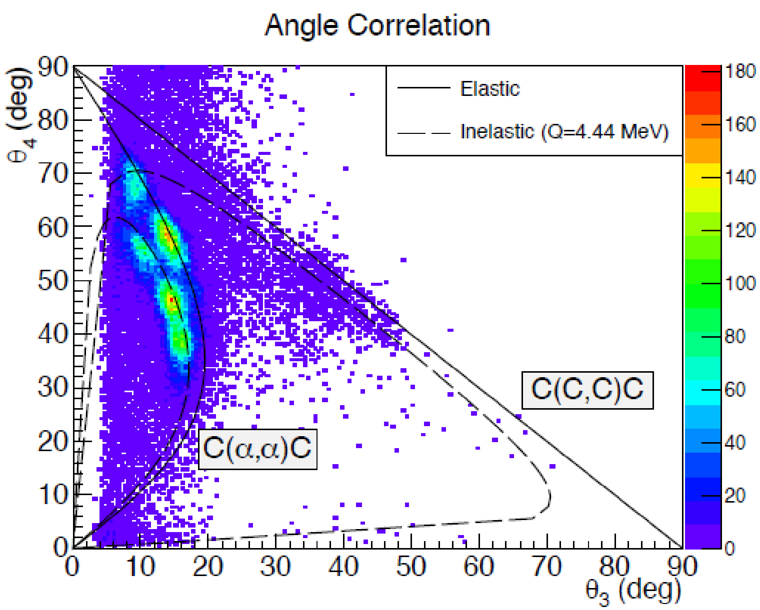

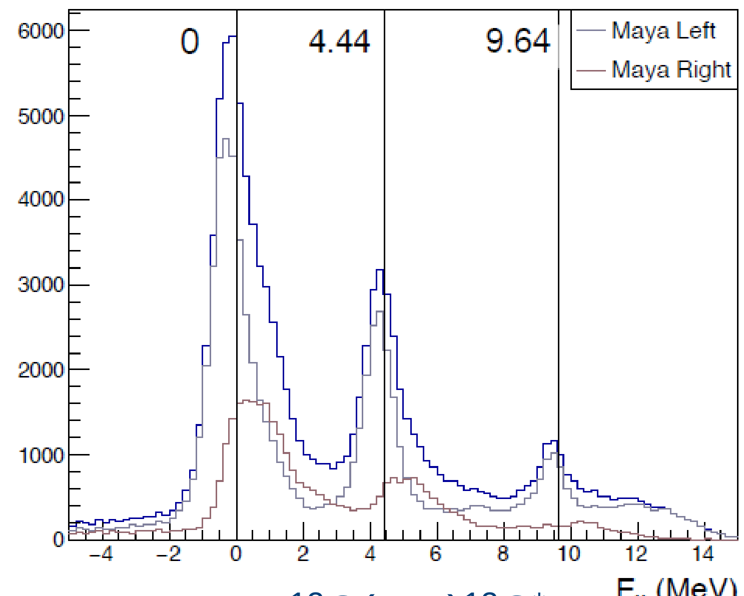

$^{12}C(\alpha,\alpha)^{12}C^{*}$

C. Wouters, Master Thesis, KU Leuven 2016

After additional work on the device

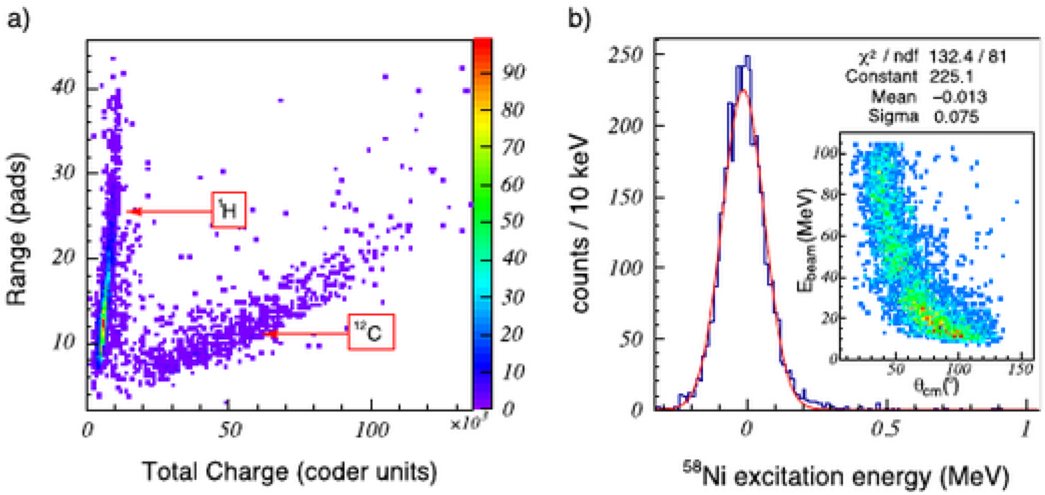

Fig. 9. (Color Online) (a) Particle identification plot obtained by correlating the range of the particles stopping in the active volume with the total charge deposit. Scattered protons and carbon ions are well separated. (b) Excitation energy spectrum reconstructed for the $^{58}Ni+p$ reaction. A Gaussian fit to this distribution (red line) results in an energy resolution of ~175 keV (FWHM). (Inset) center of mass angular and laboratory reaction energy domain covered by the present analysis.

Problem: Using heavy ion beams

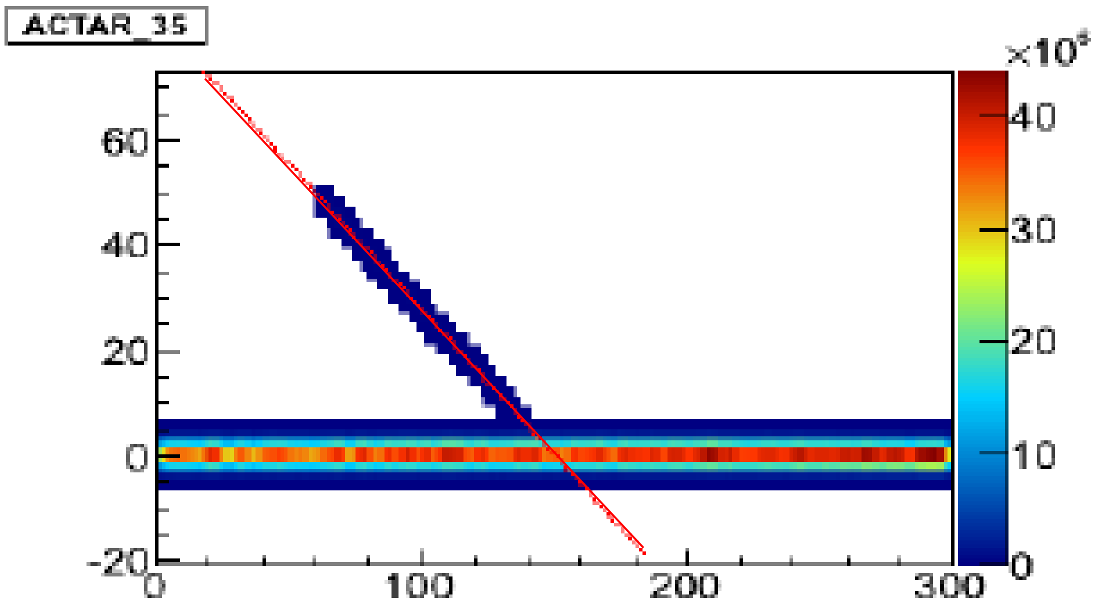

Fig. 4: Sample digitized trace for a ^{132}Sn(d,p) reaction with 2x2mm^2 sized pads. The red line corresponds to the fitted trajectory used for determining the range of the proton.

Beam Shielding

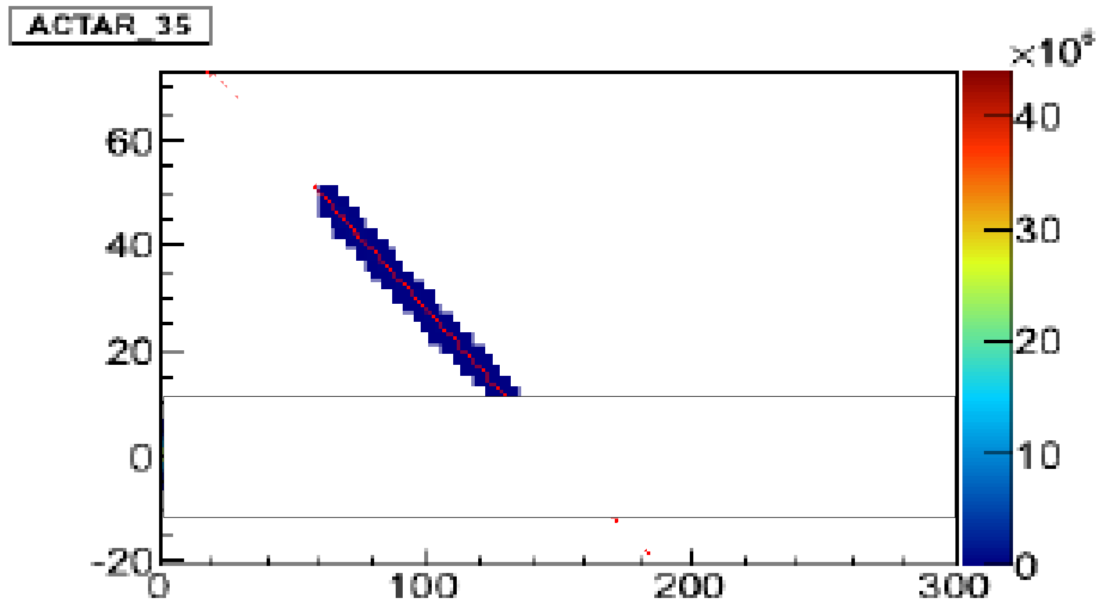

Fig. 4: Sample digitized trace for a ^{152}Sn(d,p) reaction with 2x2mm^2 sized pads. The red line corresponds to the fitted trajectory used for determining the range of the proton.

Tracking

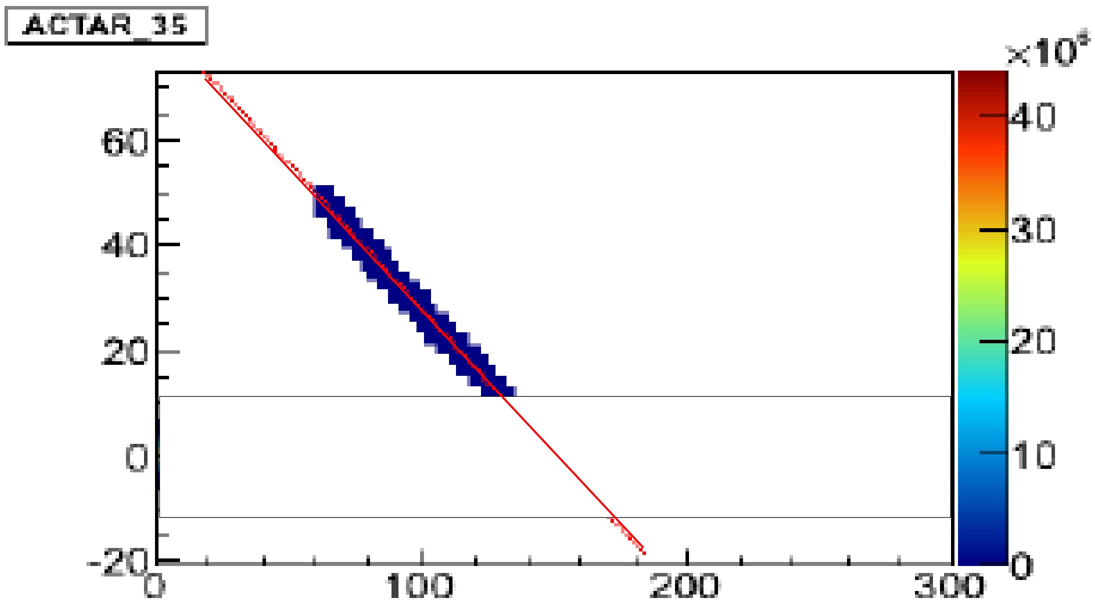

Fig. 4: Sample digitized trace for a ^{132}Sn(d,p) reaction with 2x2mm^2 sized pads. The red line corresponds to the fitted trajectory used for determining the range of the proton.

Tracking

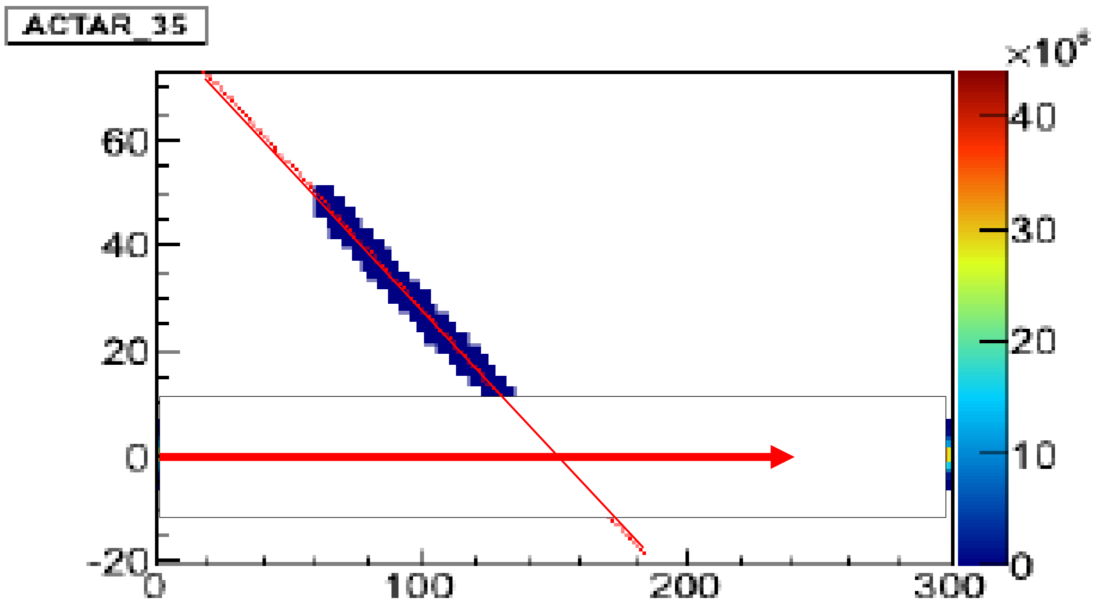

Fig. 4: Sample digitized trace for a ^{132}Sn(d,p) reaction with 2x2mm^2 sized pads. The red line corresponds to the fitted trajectory used for determining the range of the proton.

2 or more particle events

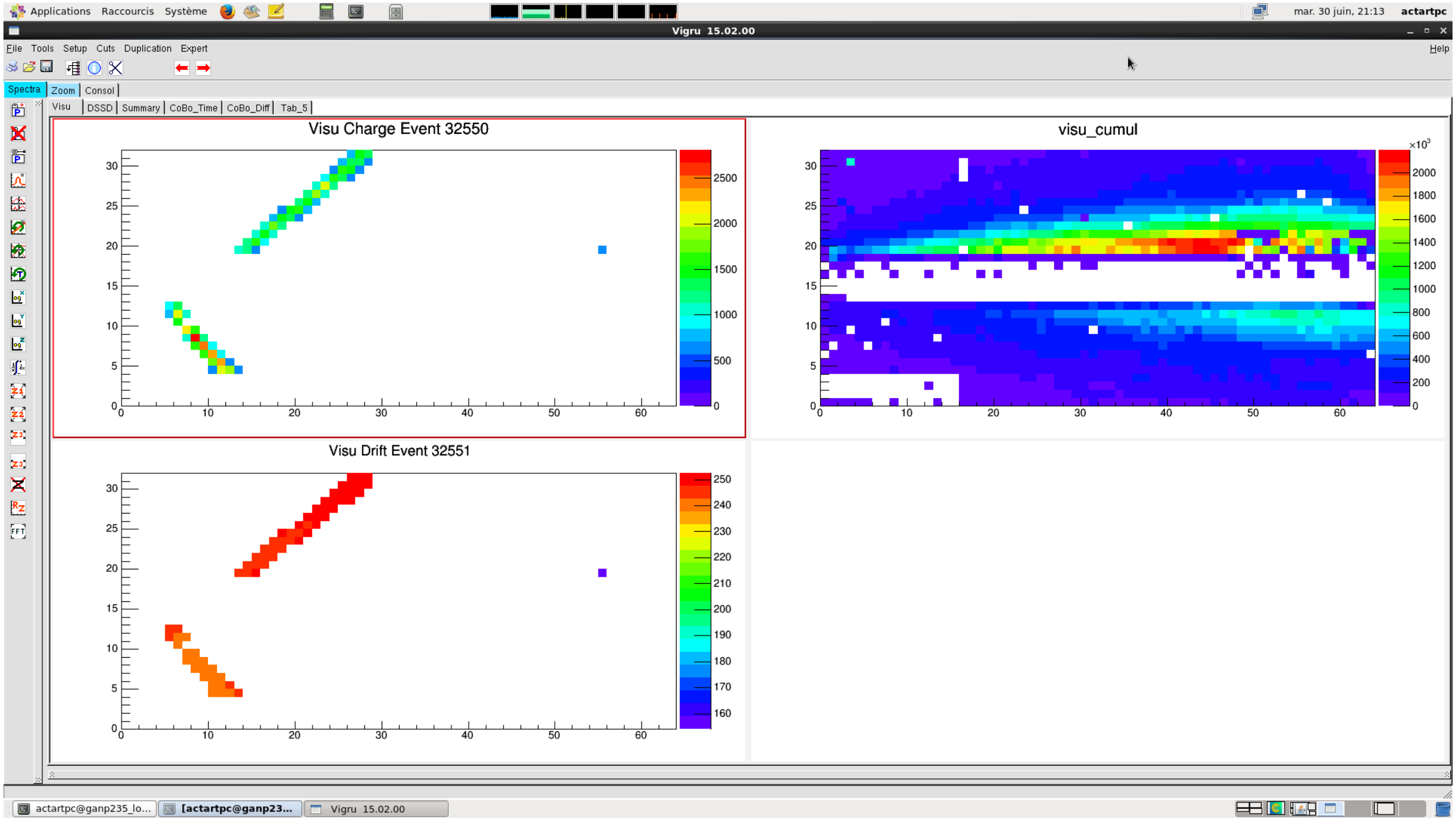

Looking for smart solutions

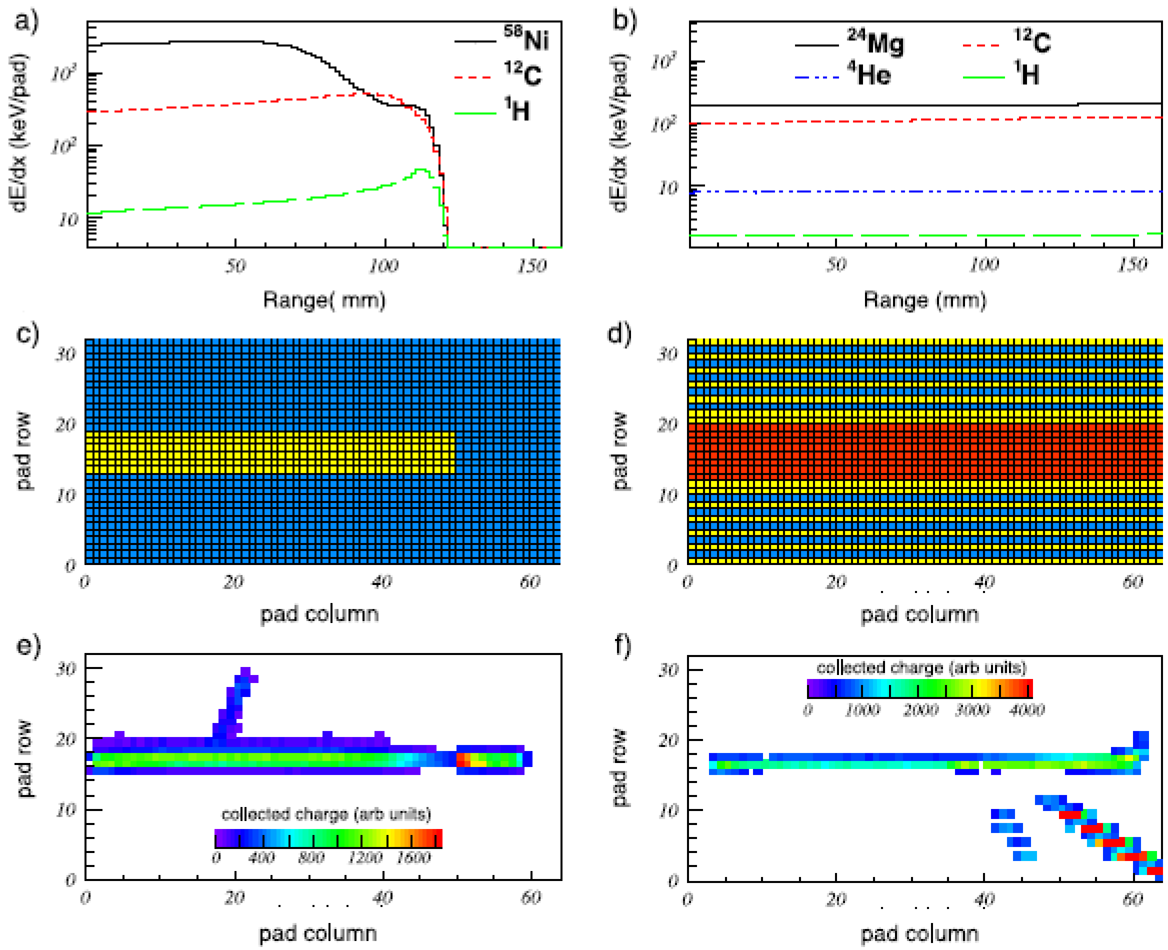

Fig. 8. (Color Online) Top: SRIM energy-loss profiles of the particles involved in the ^{58}Ni test (a) and the ^{24}Mg test (b). Middle: Gain settings applied to the pad plane for the ^{58}Ni test (c) and the ^{24}Mg test (d). Blue indicates pads with 120 fC range, yellow for 1 pC range and red for 10 pC range. Bottom: Charge projection of the scattering of a proton by a ^{58}Ni ion (e) and the scattering of a proton and ^{4}He by a ^{24}Mg ion (f).

ACTAR TPC is finally built and operational

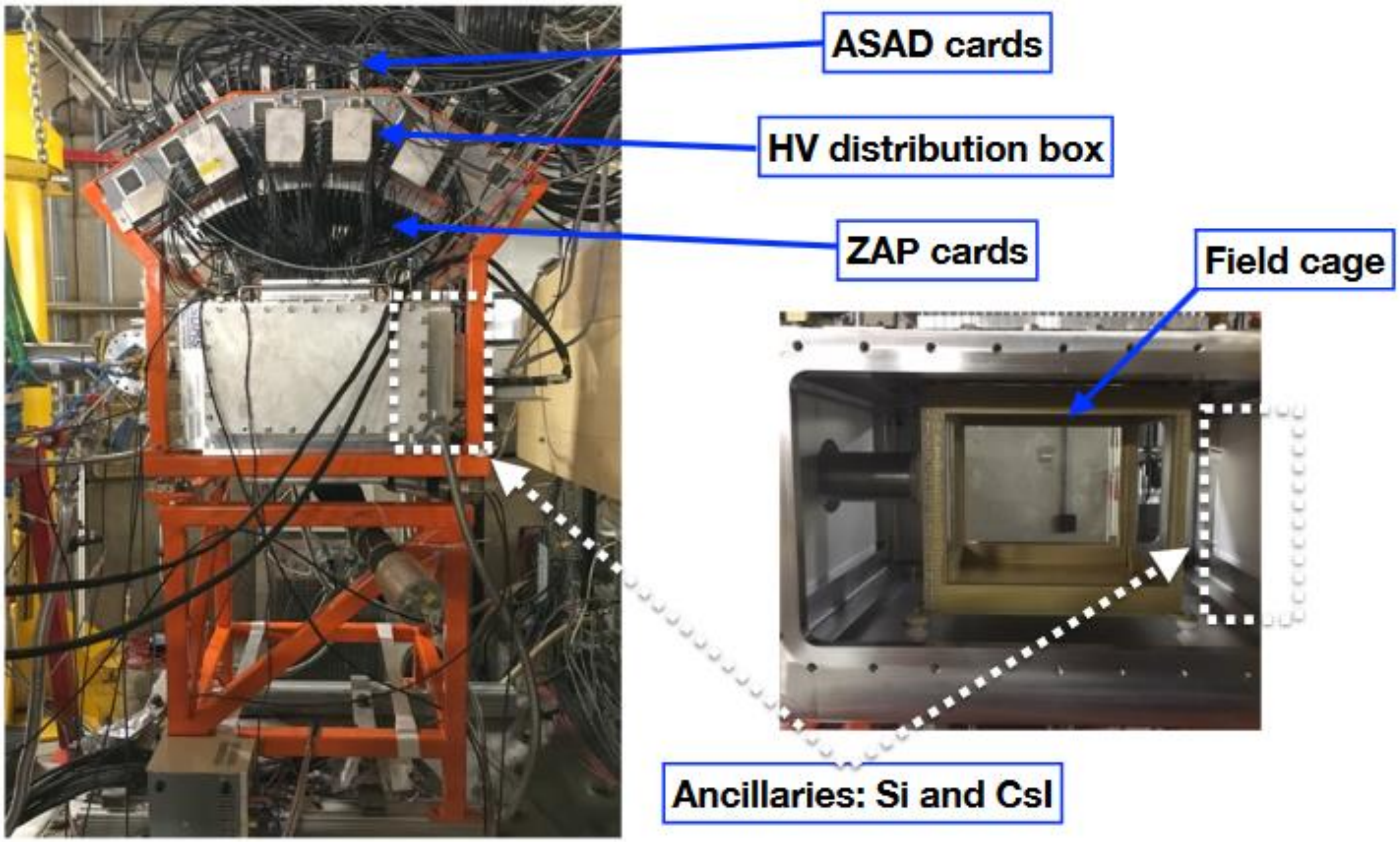

SpecMAT

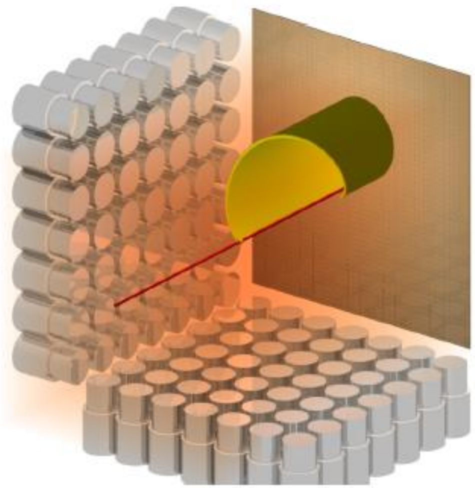

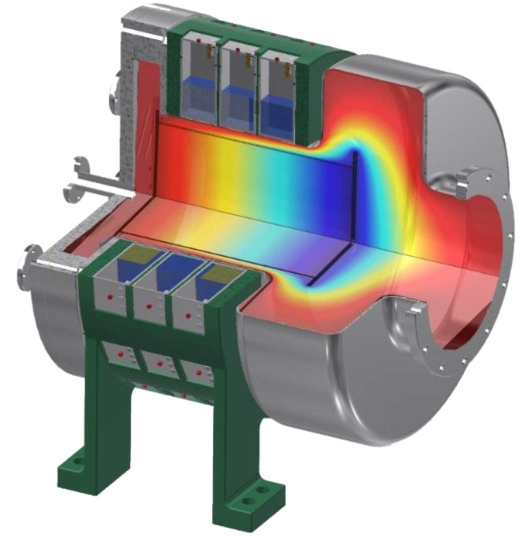

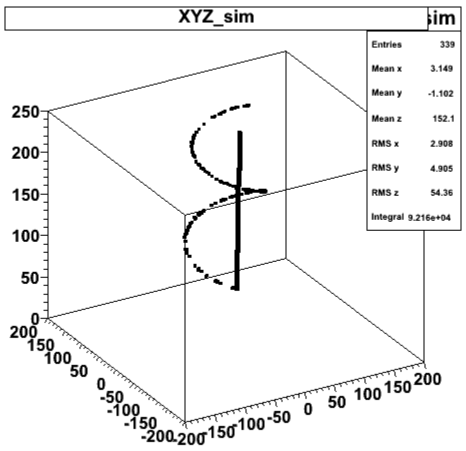
XYZ_sim
Entries 339
Mean x 3.149
Mean y -1.102
Mean z 152.1
RMS x 2.908
RMS y 4.905
RMS z 54.36
Integral 9.216e+04

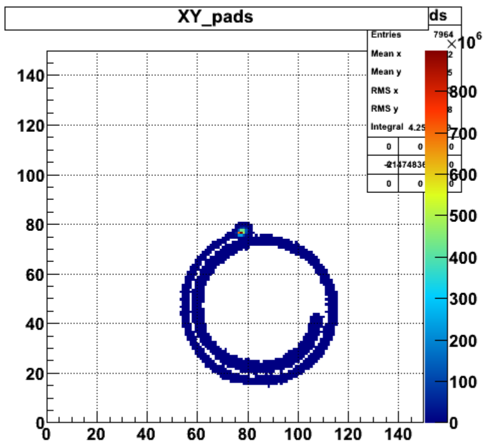
XY_pads
Entries 7964
Mean x
Mean y
RMS x
RMS y
Integral

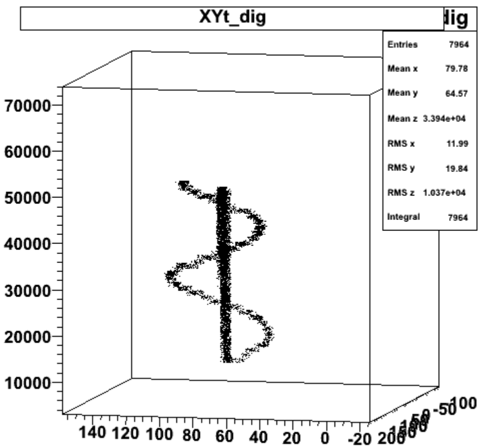
XYt_dig
Entries 7964
Mean x 79.78
Mean y 64.57
Mean z 3.394e+04
RMS x 11.99
RMS y 19.84
RMS z 1.037e+04
Integral 7964

SpecMAT - Implementation

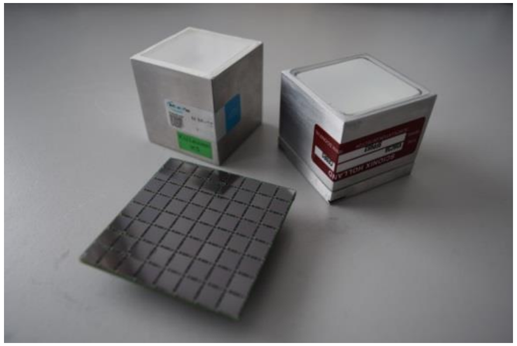

ACTIVE Target:

1. Optimize detector design: chamber radius vs gamma-ray detection efficiency
2. Develop TRACKING software
3. Mechanical design

Scintillation detector array:

1. **Optimize geometry: efficiency**
2. **Doppler correction resolution**
3. **Test detectors and electronics in high magnetic field**

Requirements:
Resolution ~3-4% @ 662 keV → $LaBr_3$, $CeBr_3$, …
Maintain high efficiency … it's an active target!
Magnetic field: use of SiPM

Caveat: Interaction point is not fixed!

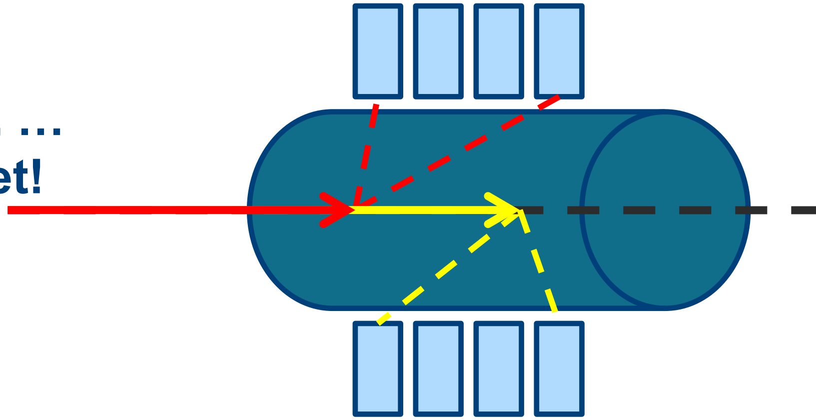

Simulations of scintillator array in GEANT4

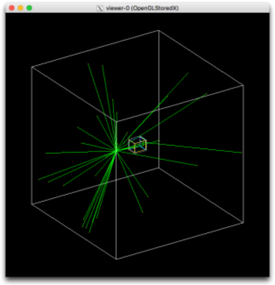

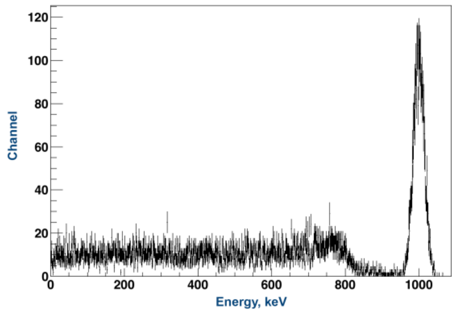

1-Comparison of simulated and experimentally measured efficiency for one 1,5”x1,5”x1,5” $CeBr_3$ crystal at 120 mm

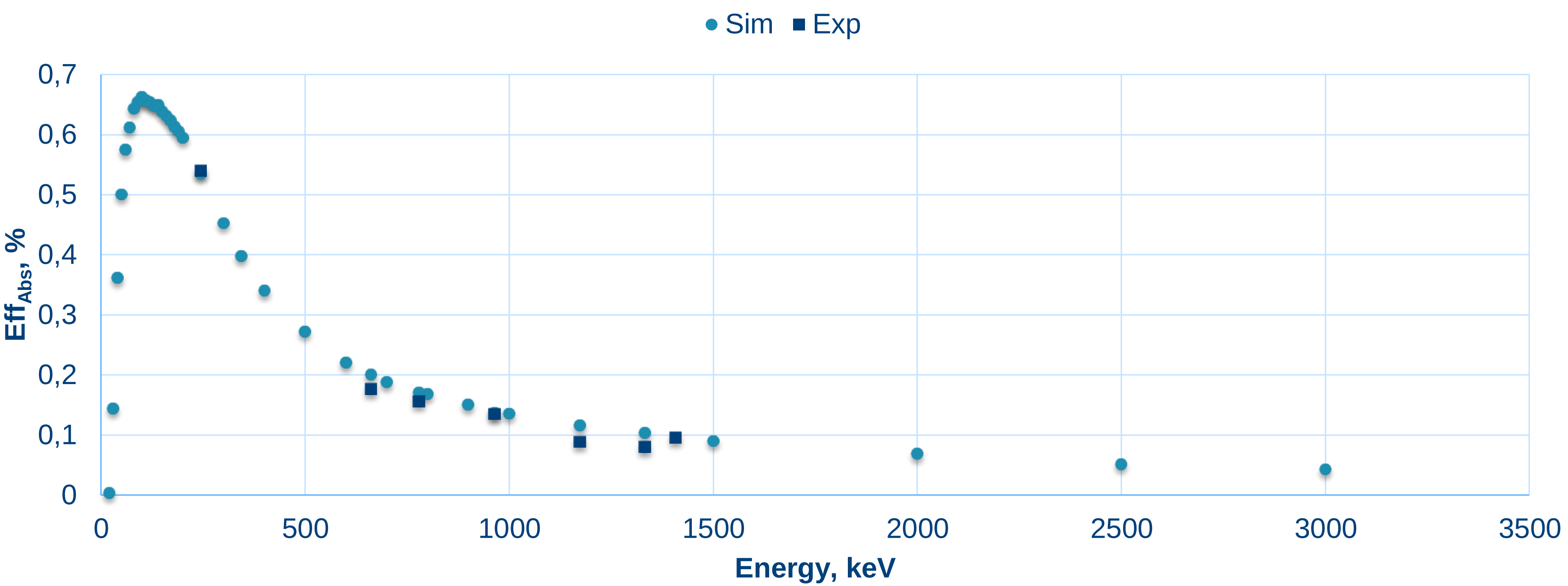

Simulation by O. Poleshchuk

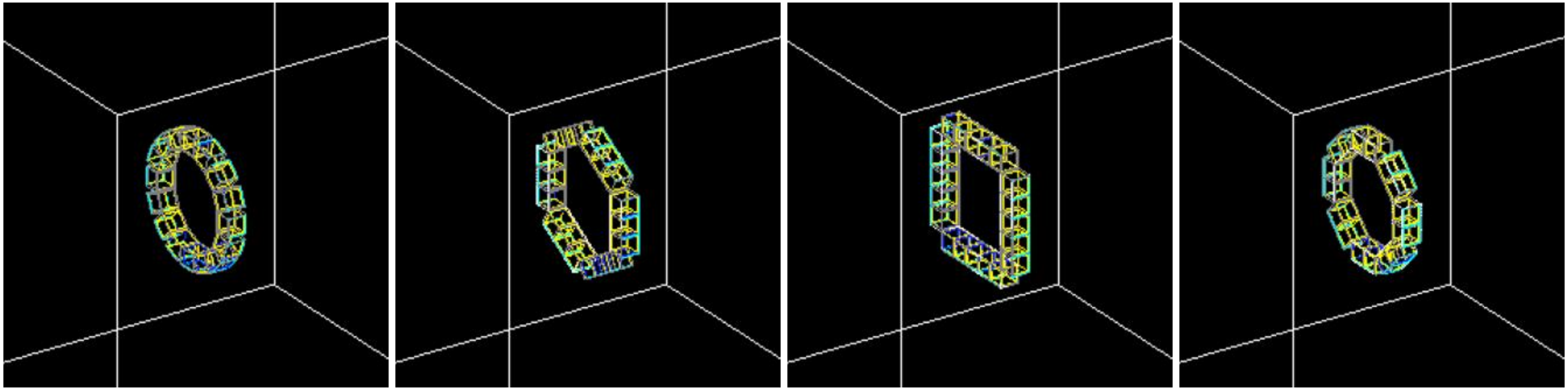

Comparison of Eff_{Abs} for different array shapes of 1,5"x1,5"x1,5" $CeBr_3$ crystals

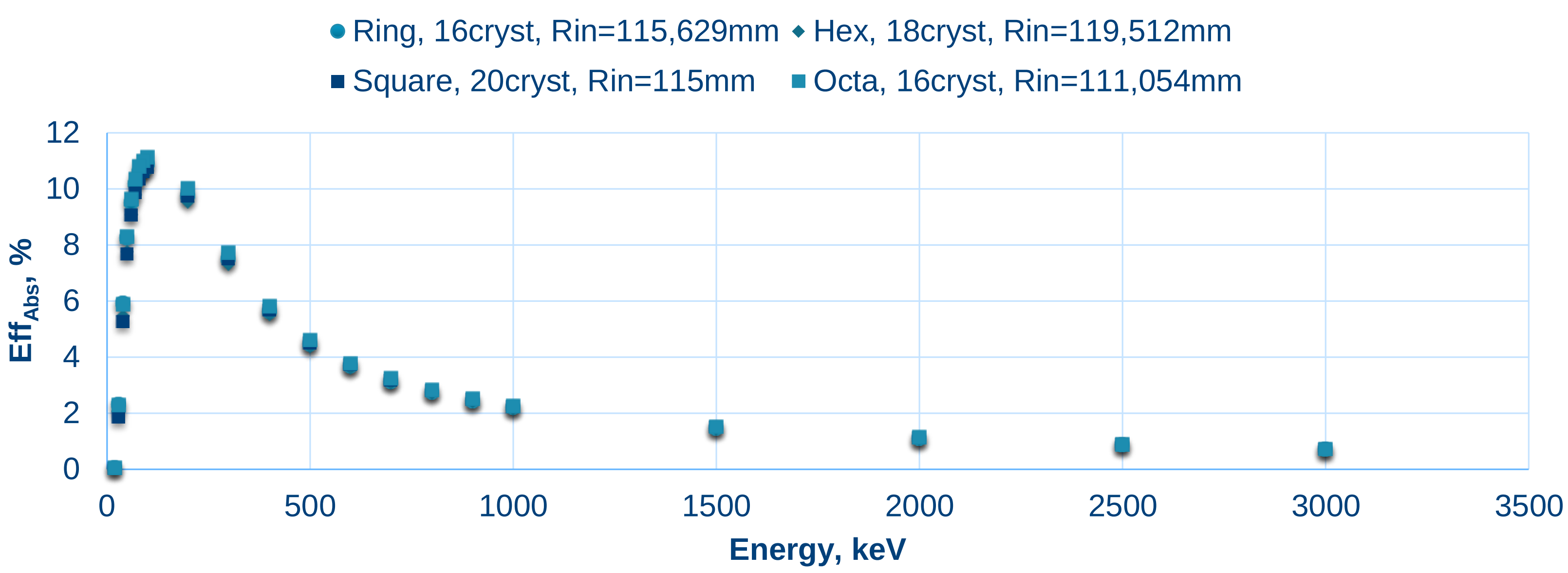

Simulation by O. Poleshchuk

Scintillation detectors test

Test at GANIL (January 2016)

- B-field up to 1,7 T
- 1.5”x1.5”x1.5” cubic $LaBr_3$
- Analogue and Reduced GET electronics

Test at UZ Leuven (August 2016)

- B-field up to 3 T
- 1.5”x1.5”x1.5” cubic $LaBr_3$:Ce and $CeBr_3$
- Analogue, CAEN and Reduced GET electronics

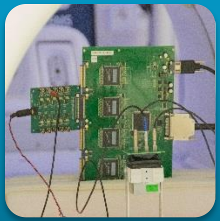

Test at UZ Leuven (August 2017)

- B-field up to 3 T
- 1.5”x1.5”x1.5” cubic $LaBr_3$:Ce
- Analogue, CAEN and **Full GET electronics**

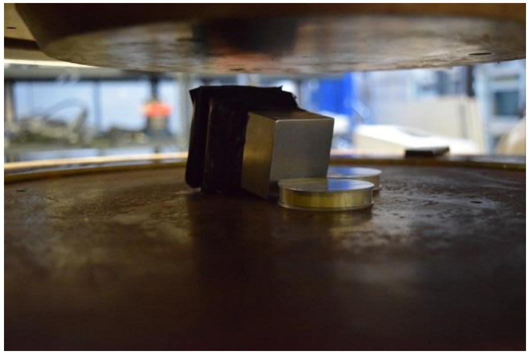

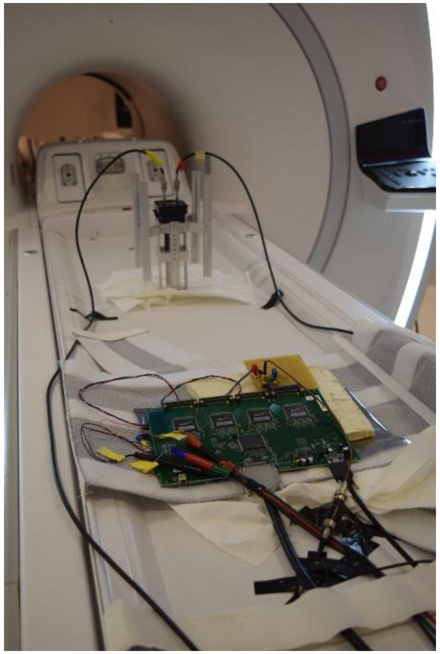

Detector and electronics tests in 3T magnetic field

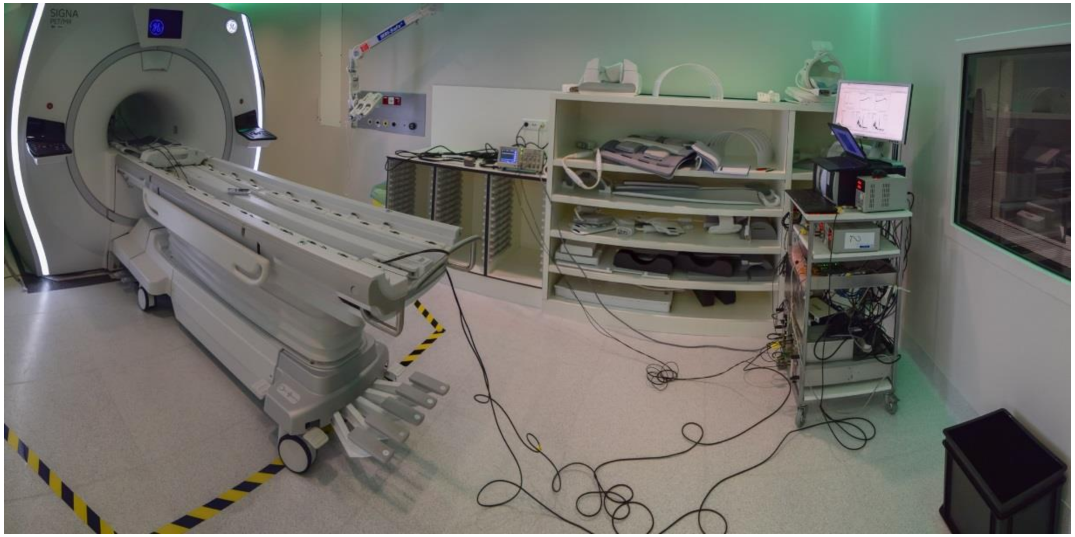

B-field

GET AsAd

Two orientations of AsAd board in the B-field

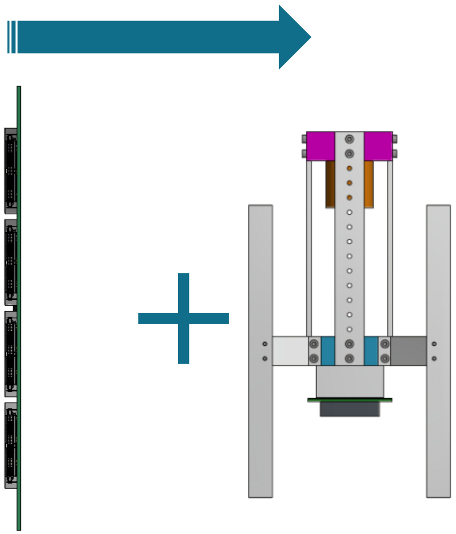

	DAQ	Analogue	CAEN	GET	GET	GET
Detector	B-field	No field	No field	No field	AsAd in 3T parallel	AsAd in 3T perpendic
$LaBr_3$+SiPM	No field	2,94±0,01%	3,22±0,01%	3,85±0,03%	3,85±0,03%	3,82±0,03%
$LaBr_3$+SiPM	3T	2,97±0,01%	3,24±0,01%	3,88±0,01%	3,85±0,01%	3,84±0,01%

Measured resolution of $LaBr_3$:Ce detector @ **661,7keV** coupled to SensL J-series Silicon Photo Multiplier and 3 different DAQ systems in “no” magnetic field region(~0,001T) and in 3T magnetic field region.

Scintillation detectors for SpecMAT

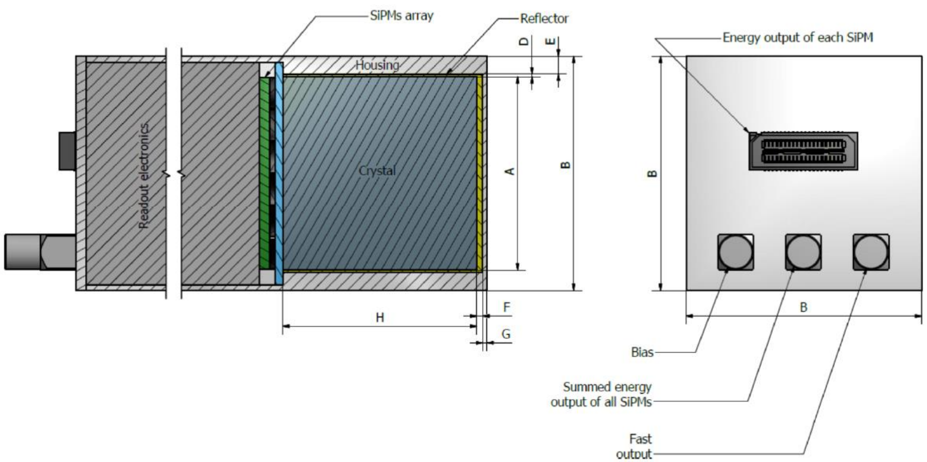

Fig. 1 Schematic drawing of the scintillation detector

SCIONIX
Dedicated Scintillation Detectors

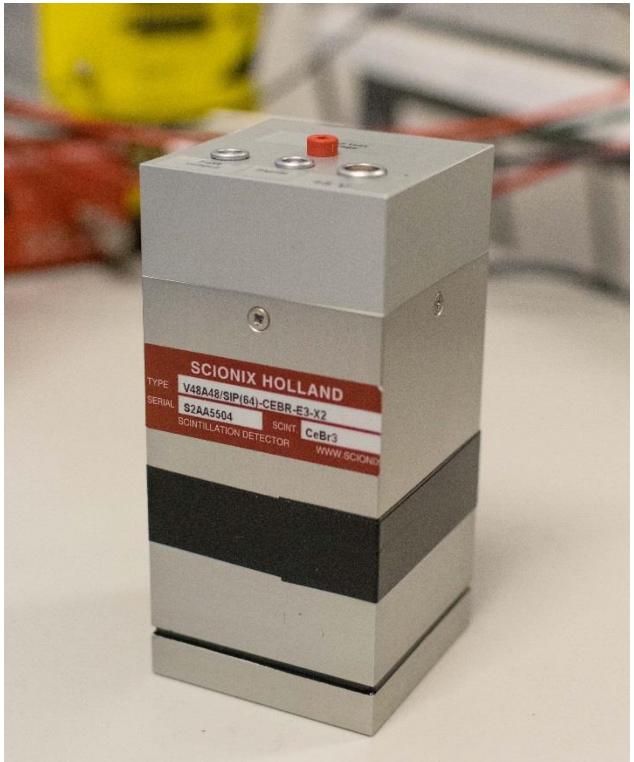

- Temperature compensated bias generator
- Built-in preamp
- $CeBr_3$ scintillator
- ~3.9% FWHM resolution @ 662keV

Design of SpecMAT

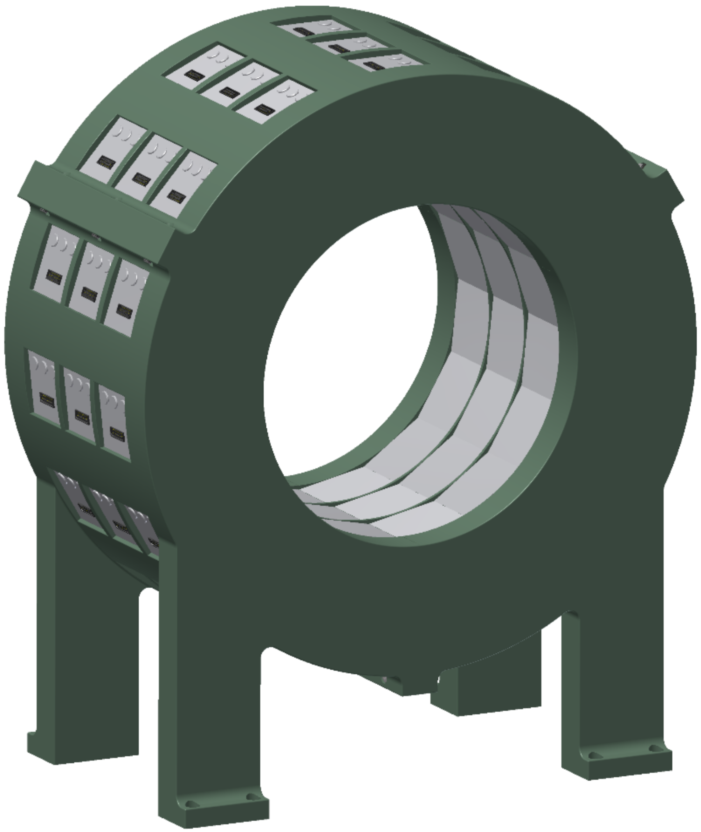

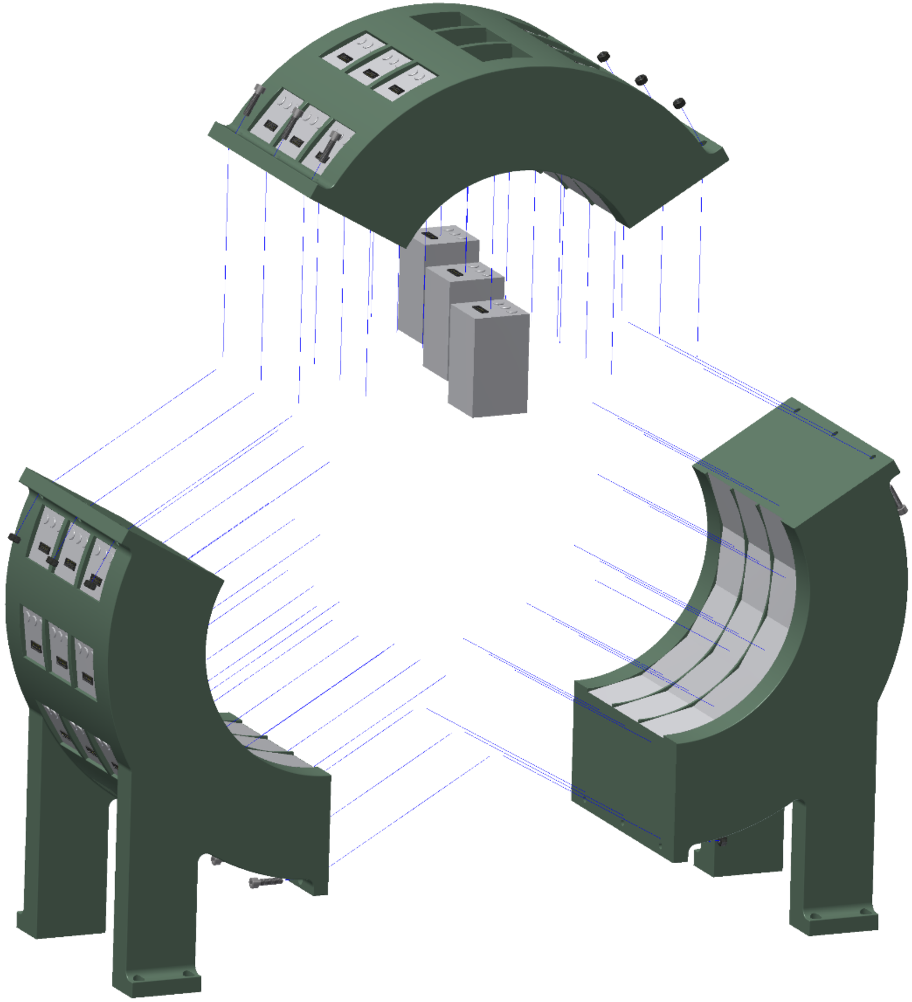

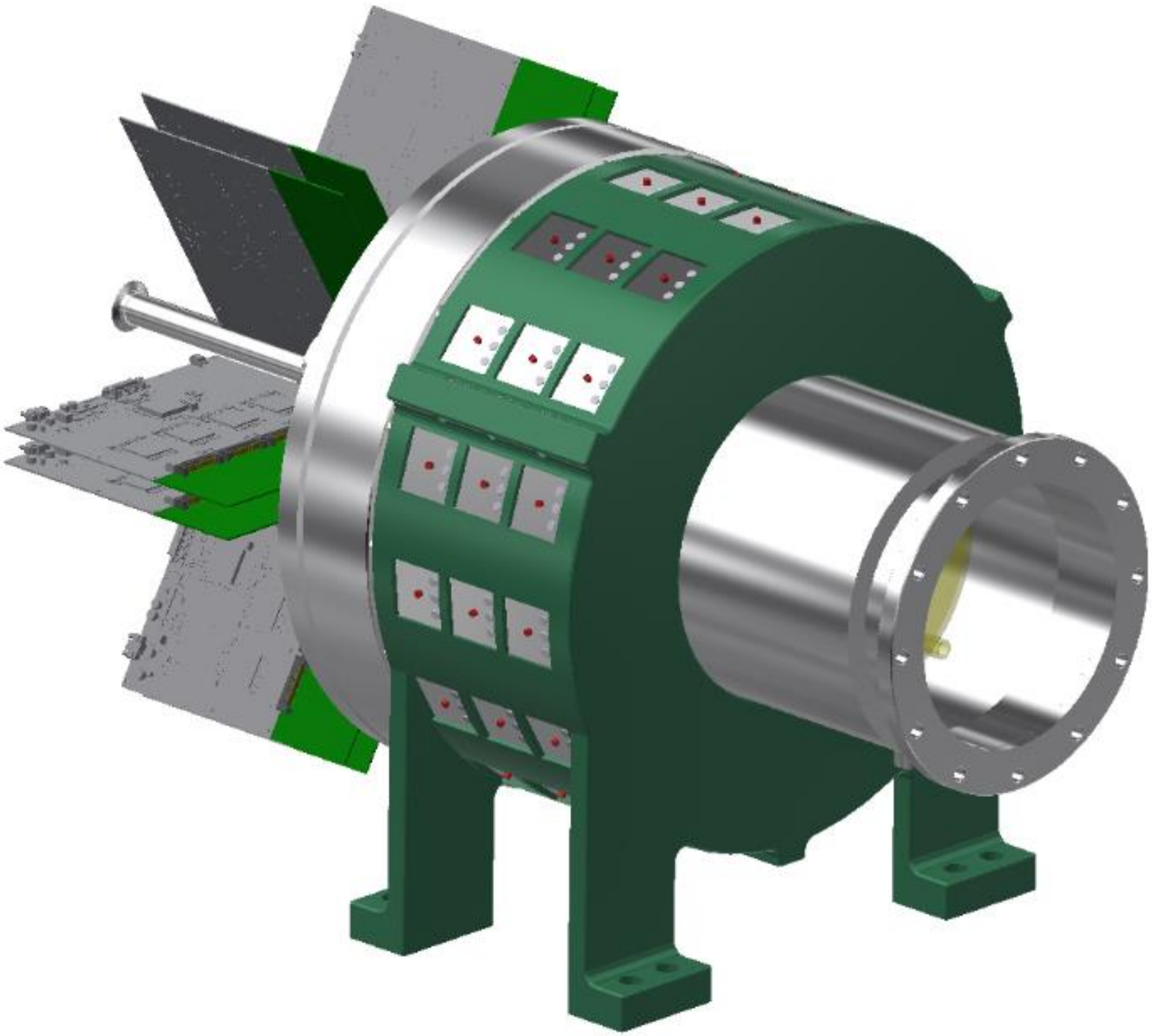

- Outlook: the near future at LNL/LNS for the ACTAR Demonstrator

Energy loss measurement

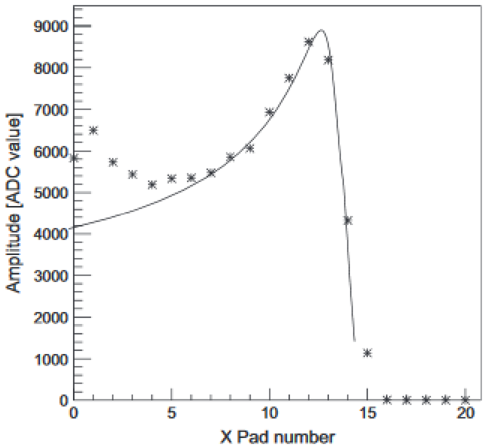

Fig. 5. Amplitude signals versus track length and expected distribution from SRIM for a 5.5 MeV alpha in 1100 mbar of Ar+CF$_4$(5%).

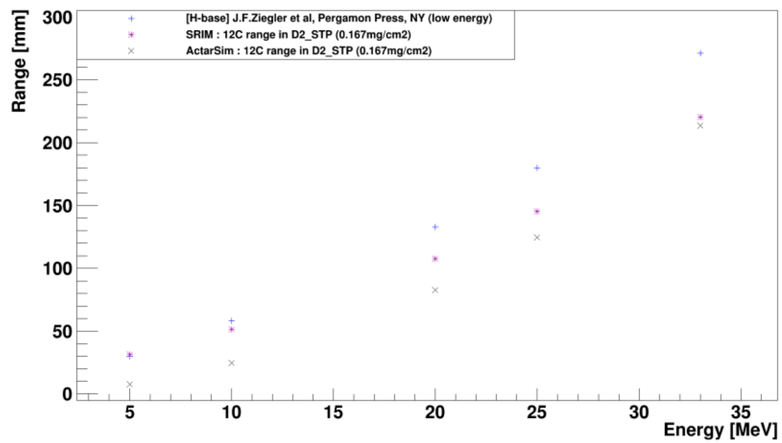

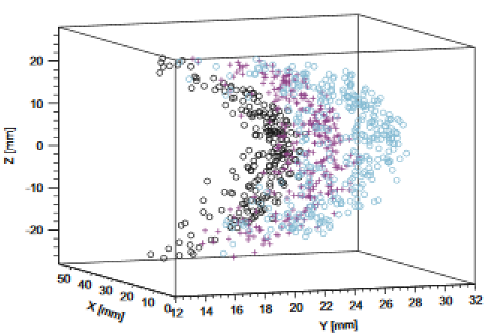

Fig. 6. Plot of the reconstructed ranges for the 3 α-particles (black Pu, red Am and blue Cm). (For interpretation of the references to color in this figure caption, the reader is referred to the web version of this article.)

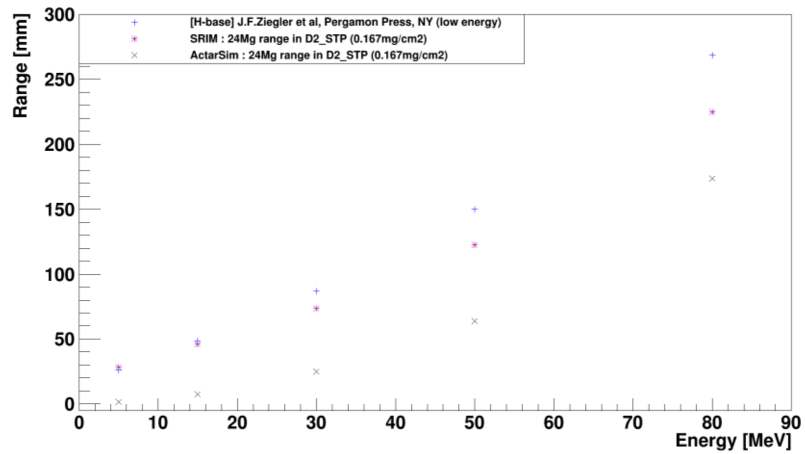

J. Pancin et al, NIM A 735 (2014)

https://github.com/ActarSimGroup/Actarsim/

Table 1. List of the proposed projectile for the energy loss profile measurements. As an example, the pressure needed to stop the gas on the pad plane is given for the iC_4H_{10} case.

Ion	Beam Energy (MeV/u)	Gases to be measured	BTU requested	*iC4H10 pressure (mbar) typical case example*
^{7}Li	1.0 - 4.5	H_2, D_2, CH_4, iC_4H_{10}, CF_4, CO_2, He	4.5	*500*
^{9}Be	1.5 - 4.5		4.5	*500*
^{10}B	1.8 - 4.5		4.5	*500*
^{12}C	2.0 - 4.5		4.5	*250*
^{15}N	2.0 - 4.5		4.5	*250*
^{16}O	2.0 - 4.5		4.5	*250*
^{19}F	2.0 - 4.5		4.5	*250*
^{24}Mg	2.0 - 4.5		4.5	*250*
^{40}Ca	2.0 - 3.8		4.5	*250*
^{120}Sn	1.5 - 1.7		4.5	*125*
Total			45	

Test case: $^{19}F(p,a)$ reaction at E_p=5-7 MeV (TANDEM)

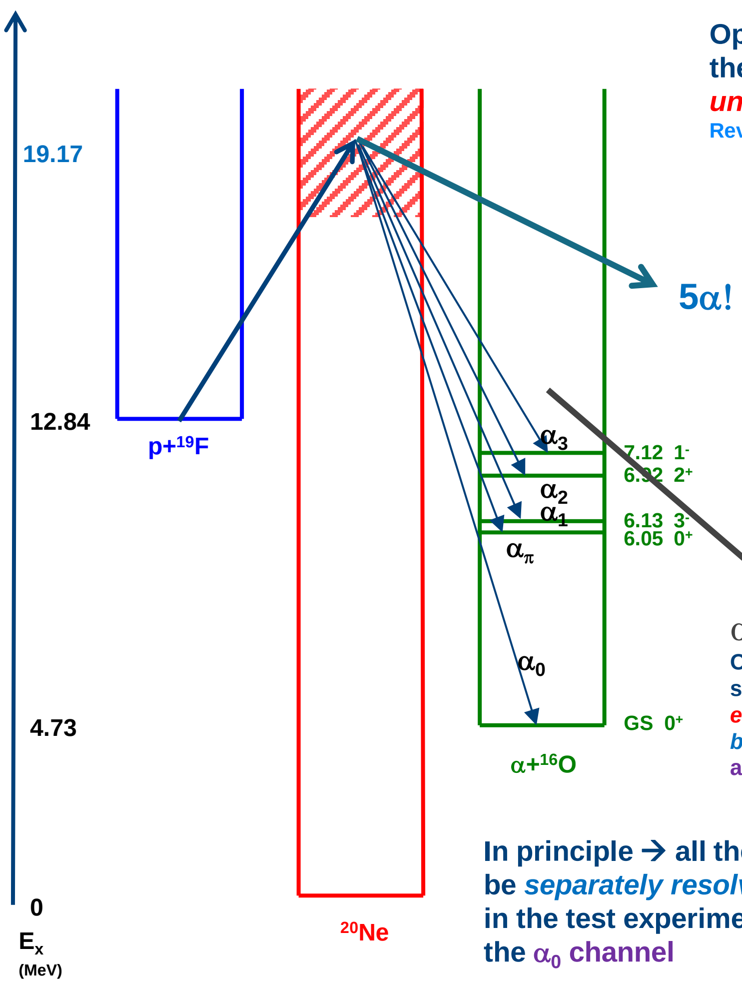

Opportunity to measure with *good accuracy* the angle-integrated *cross section* → large *uncertainties* at E_p=5-7 MeV (Warsh et al, Phys. Rev. 131 (1963) 1690)

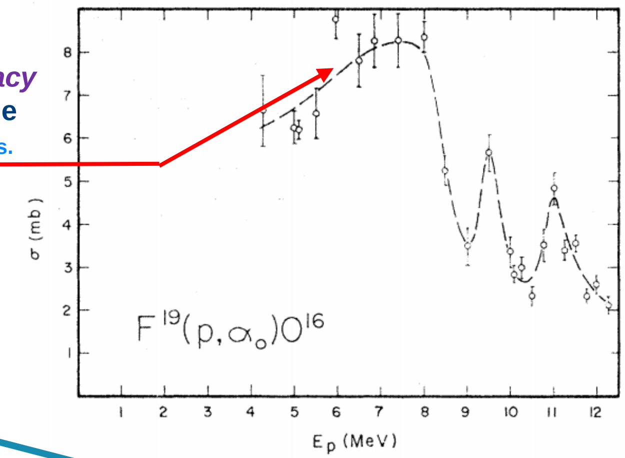

Ambiguities in *shapes* and in the absolute *x-section scale* of angular distributions
(Warsh et al, Phys. Rev. 131 (1963) 1690)

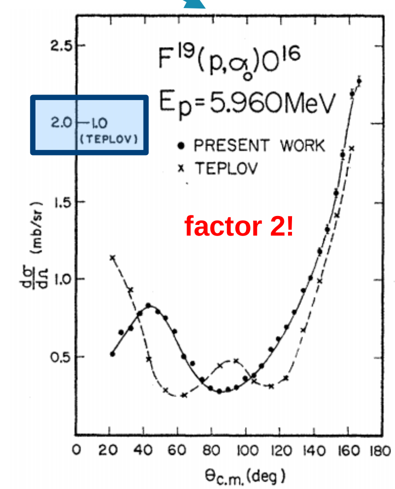

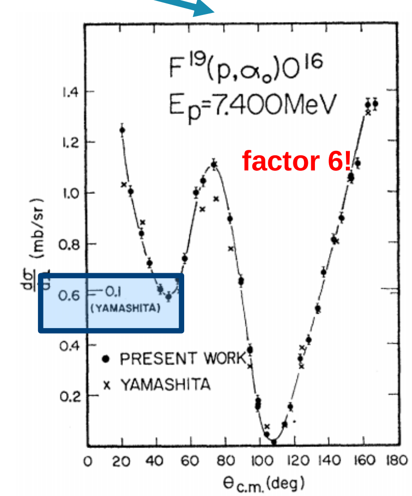

α feeding:
Opportunity of studying *multi-track events* with *low background* and no ambiguities

In principle → all the α_i channels can be *separately resolved* (to be verified in the test experiment) → surely for the α_0 channel

Test case 2: ^{120}Sn(d,p) reaction at E_{Sn}= 15 AMeV (CS)

Schneid et al, Phys Rev 156 (1967) 4

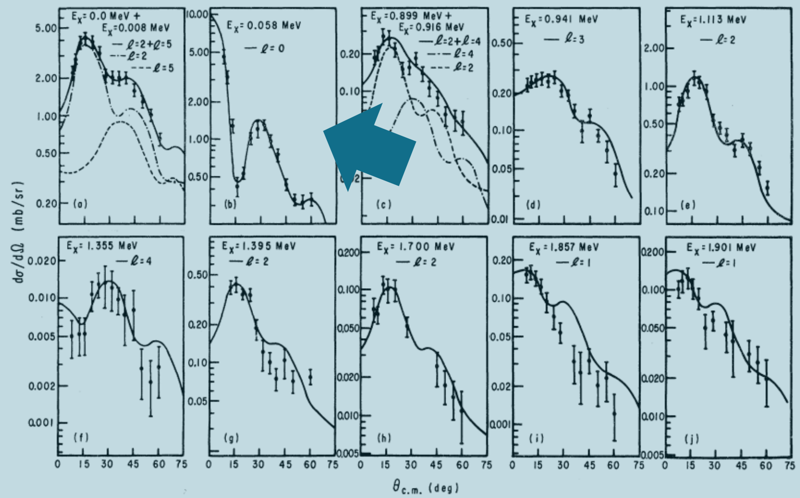

FIG. 2. Angular distributions of transitions in the ^{120}Sn$(d,p)^{121}$Sn reaction. The experimental points are given with error bars corresponding to statistics and background subtraction. The solid lines are DWBA curves fitted to the experimental data.

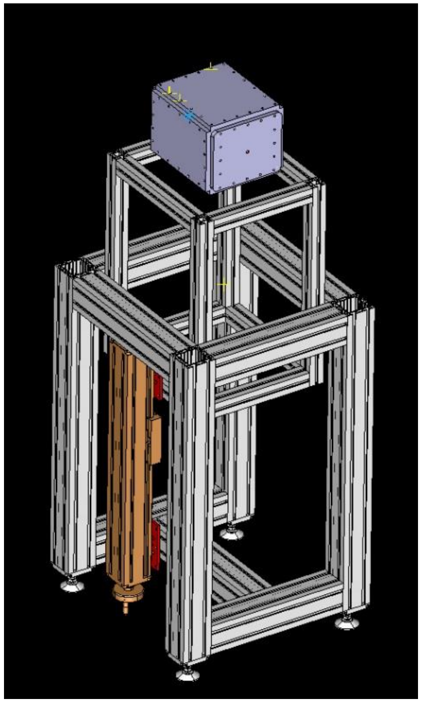

Figure 4: A schematic view of the second detection stage of OSCAR. The rear board contains two series of 8 compact charge sensitive pre-amplifiers to collect signals from 16 silicon pads welded on the front board.

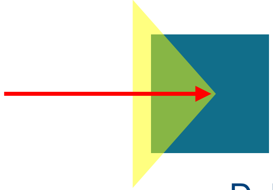

D. Dell'Aquila, NIM A 877 (2018) 227

<u>Auxiliary detectors:</u>
-Si Strip Pads (BB7)
-OSCAR-like Si pins
-SPECMAT CeBr3

<u>Challenges:</u>
-High density of states
-Kinematics reconstruction

Development of tracking codes

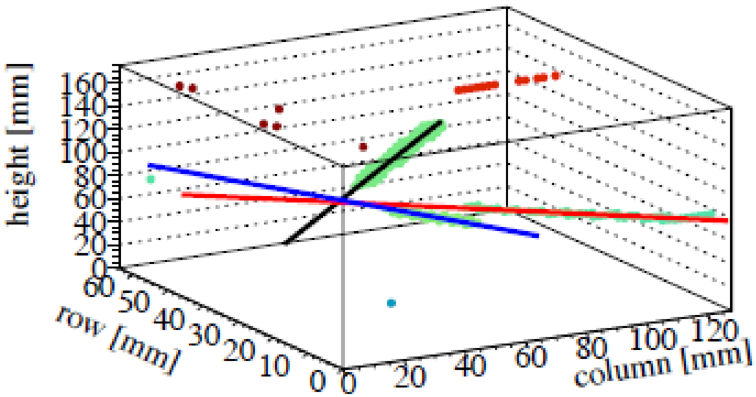

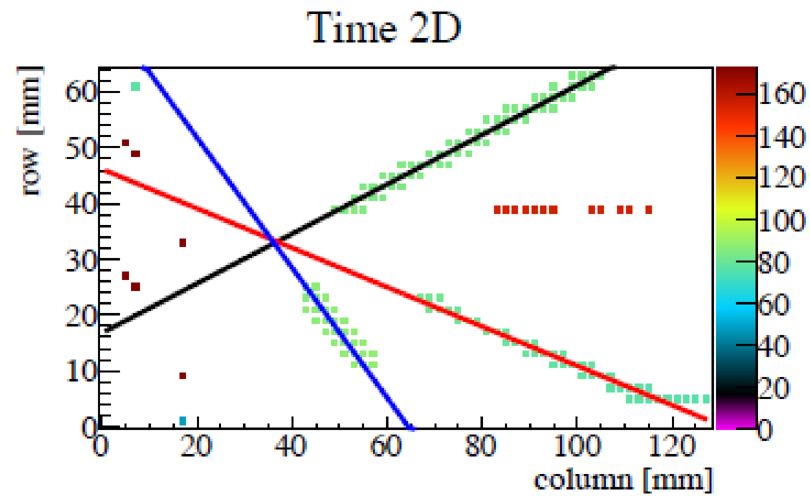

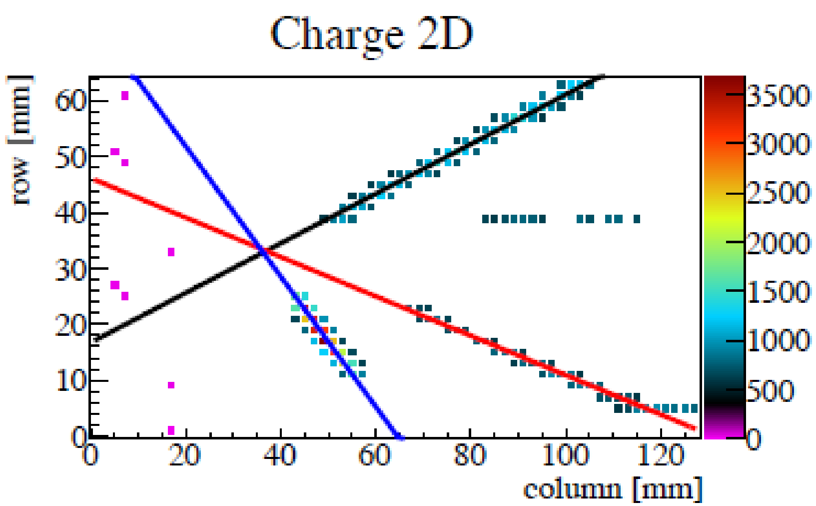

TFile : RANSAC3Dv4.root
TTree : Track3, Event # 1
Original Event # 5

RANSAC Information
MAXLOOP : 2000
THRESHOLD : 12000
WIDTH : 5.00

Courtesy of K. Hagiwara (Okayama University and Unipd)

Beyond MagicTin: physics opportunities with an active target at SPES

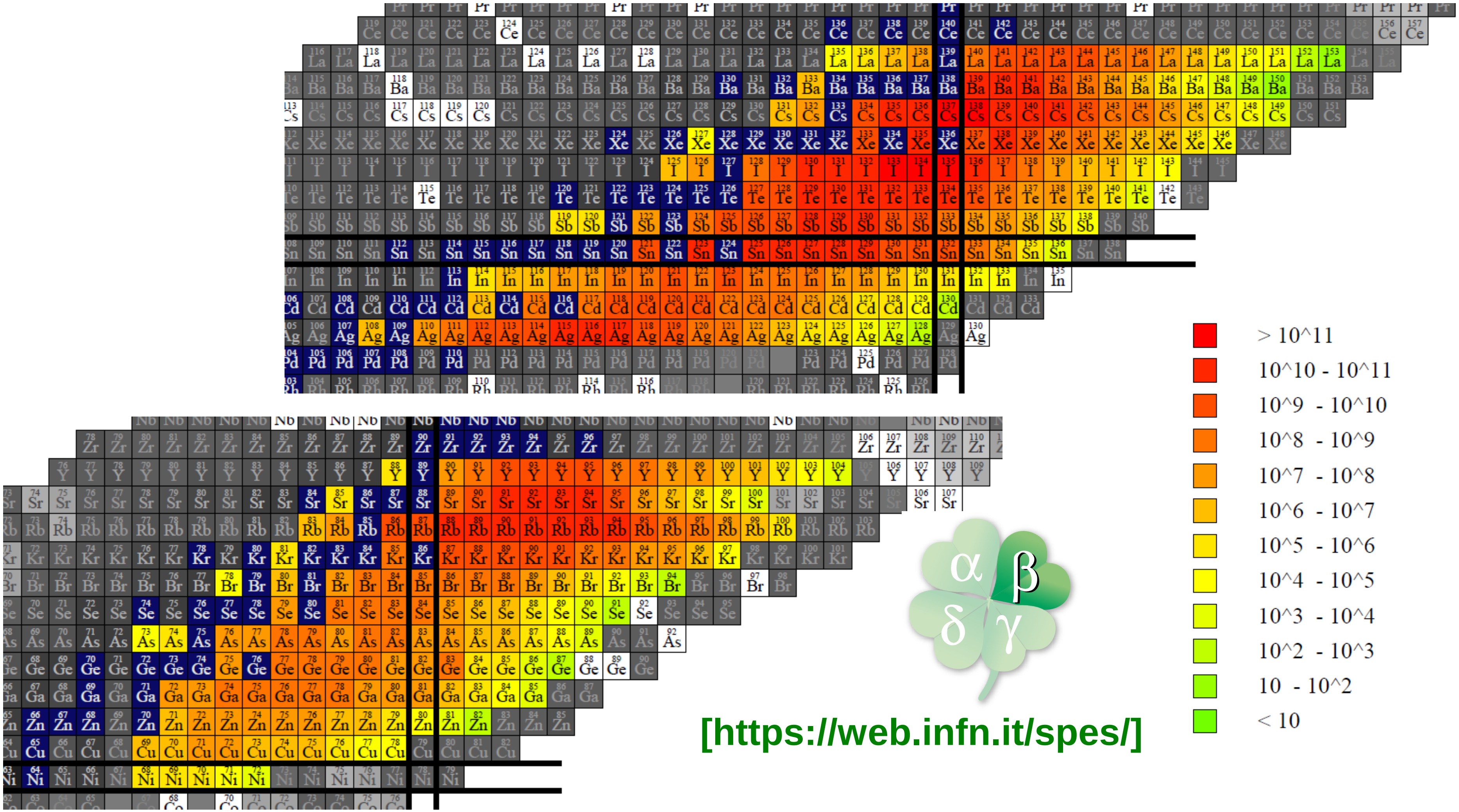

[https://web.infn.it/spes/]

Two letters of intent for SPES endorsed by the SAC:
B. Fernandez Dominguez et al, Direct Reactions with exotic nuclei in the r-process using an active target
R. Raabe, T. Marchi et al, Shell Structure in the vicinity of ^{132}Sn with an active target

Summary

- Active Targets are promising tools for studying Clustering effects in exotic nuclei and the Nuclear EoS at low density
- Several projects are ongoing worldwide
- In Europe ACTAR TPC and SpecMAT are focusing also on clustering and EoS
- ACTAR TPC based on the MAYA and ACTAR Demonstrator experiences is ready for experiments at GANIL
- We will continue using the demonstrator for further R&D towards SPES

GDS: GAS-FILLED DETECTORS AND SYSTEMS

HOME MEETINGS COLLABORATION PROJECTS NEWS & DOCUMENTS CONTACT US

ENSAR2

Gas-Filled Detectors and Systems. Network Activity in ENSAR2

http://igfae.usc.es/gds

Task 1: gather together the GDS community

4 topical meetings

Task 2: Auxiliary detectors

Task 3: Novel detection systems for high-intensity and heavy beams

Task 4: Rare gas target handling and recycling systems

Task 5: GDS in strong and non-uniform magnetic fields

ACTAR TPC and NUCLEX collaborations

H. Alvarez-Pol[6], P. Ascher[7], M. Babo[2,8], S. Barlini[9], B. Bastin[3], M. Bini[9], B. Blank[7], M. Bruno[10], M. Caamaño[6], G. Casini[9], A. Camaiani[9], A. Chbihi[3], S. Ceruti[2], G. Collazuol[11,12], M. Cinausero[1], D. Dell'Aquila[15], D. Fabris[11], M. D'Agostino[10], F. de Oliveira Santos[3], N. de Sereville[8], H. De Witte[2], B. Duclos[3], Q. Fable[3], B. Fernandez-Dominguez[6], F. Flavigny[8], A. Gottardo[1], M. Gerbaux[7], J. Giovinazzo[7], T. Goigoux[7], F. Gramegna[1], S. Grévy[7], G.F. Grinyer[4], J. Grinyer[4], D. Gruyer[16], F. Hammache[8], T. Kurtukian-Nieto[2], B. Mauss[3], M. Mazzocco[11,12], D. Mengoni[11,12], I. Lombardo[5], L. Morelli[3,10], P. Morfouace[3], P. Ottanelli[9], G. Pasquali[9], J. Pancin[3], S. Piantelli[9], J. Pibernat[2], E.C. Pollacco[13], O.Poleshchuk[2], R. Raabe[2], T. Roger[3], M. Renaud[2], A.A. Raj[2], F. Saillant[3], P. Sizun[13], I. Stefan[8], D. Suzuki[14], J.J. Valiente-Dobòn[1], S. Valdrè[9], G. Verde[5], G. Wittwer[3], J. Yang[2].

[1]INFN, Laboratori Nazionali di Legnaro, Viale Dell'Università, 2 – 35020 Legnaro (PD), Italy ● [2]KU Leuven, Instituut voor Kern- en Stralingsfysica, Celestijnenlaan 200D, 3001 Leuven, Belgium ● [3]GANIL, CEA/DRF-CNRS/IN2P3, Bvd Henri Becquerel, 14076 Caen, France ● [4]Univ of Regina, Regina, Canada ● [5]INFN, Sezione di Catania, Catania, Italy ● [6]Universidade de Santiago de Compostela, 15706 Santiago de Compostela, Spain ● [7]CENBG, Université Bordeaux 1, CNRS/IN2P3, Chemin de Solarium, 33175 Gradignan, France ● [8]IPN Orsay, CNRS/IN2P3, Université Paris-Sud, Université Paris-Saclay, 91406 Orsay, France ● [9]INFN, Sezione di Firenze and Università di Firenze, Firenze, Italy ● [10]INFN, Sezione di Bologna and Physics and Astronomy department, University of Bologna, Bologna, Italy ● [11]INFN, Sezione di Padova, Padova, Italy ● [12]Dipartimento di fisica e Astronomia dell'Università di Padova, Via Marzolo 8, Padova, Italy ● [13]CEA, Centre de Saclay, IRFU/SPhN 91191 Gif-sur-Yvette, France ● [14]RIKEN Nishina Center, 2-1 Hirosawa, Wako, Saitama 351-0198, Japan ● [15]National Superconducting Cyclotron Laboratory, Michigan State University, East Lansing, Michigan 48824, USA ● [16]Laboratoire de Physique Corpusculaire de Caen, 6 Bvd du maréchal Juin 14050 CAEN CEDEX 4, France.

Beyond MagicTin: physics opportunities with an active target at SPES

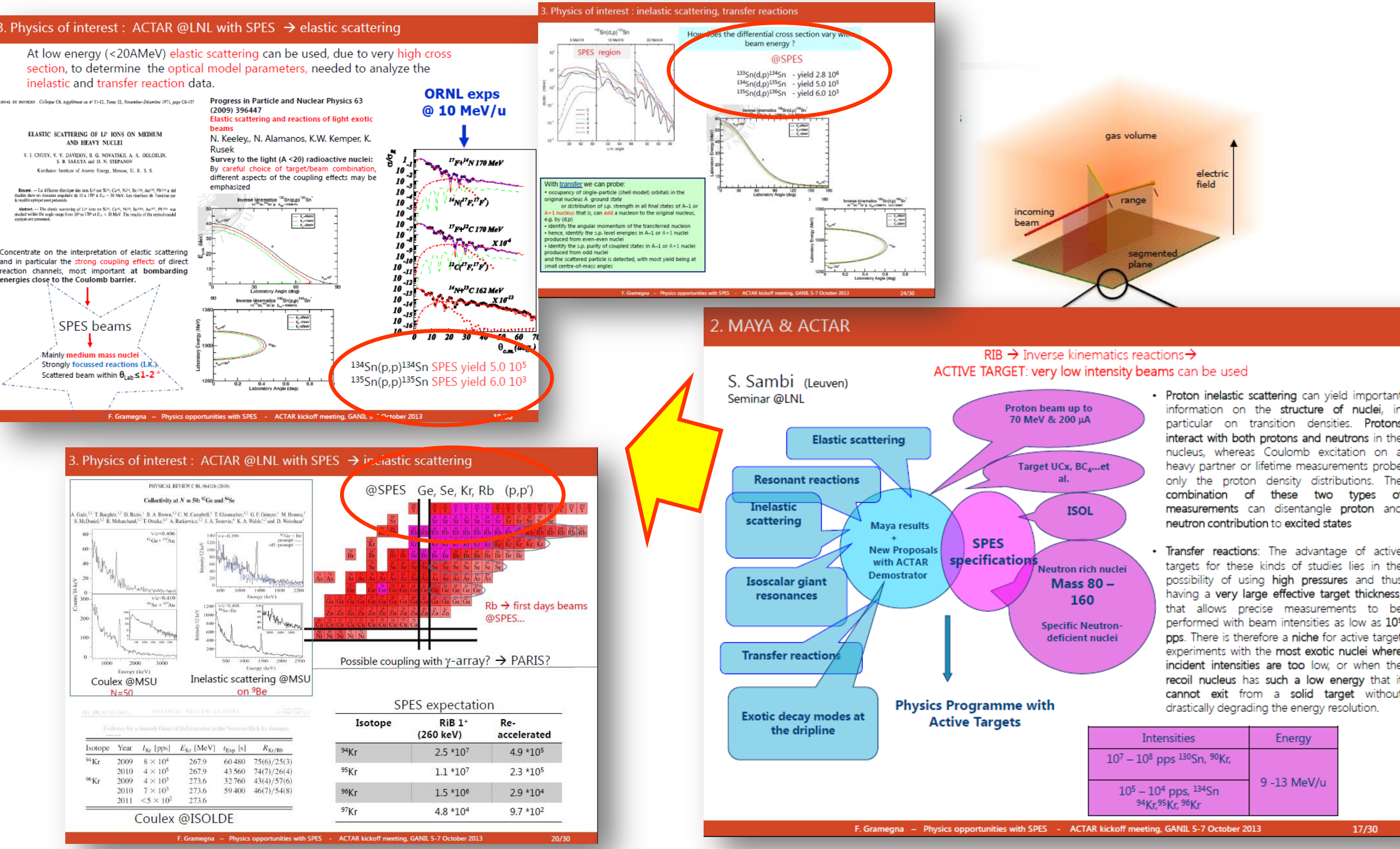

[F. Gramegna, ACTAR TPC Kickoff meeting 2013]

MagicTin

MARIE CURIE ACTIONS

Shell evolution and collectivity in Tin isotopes

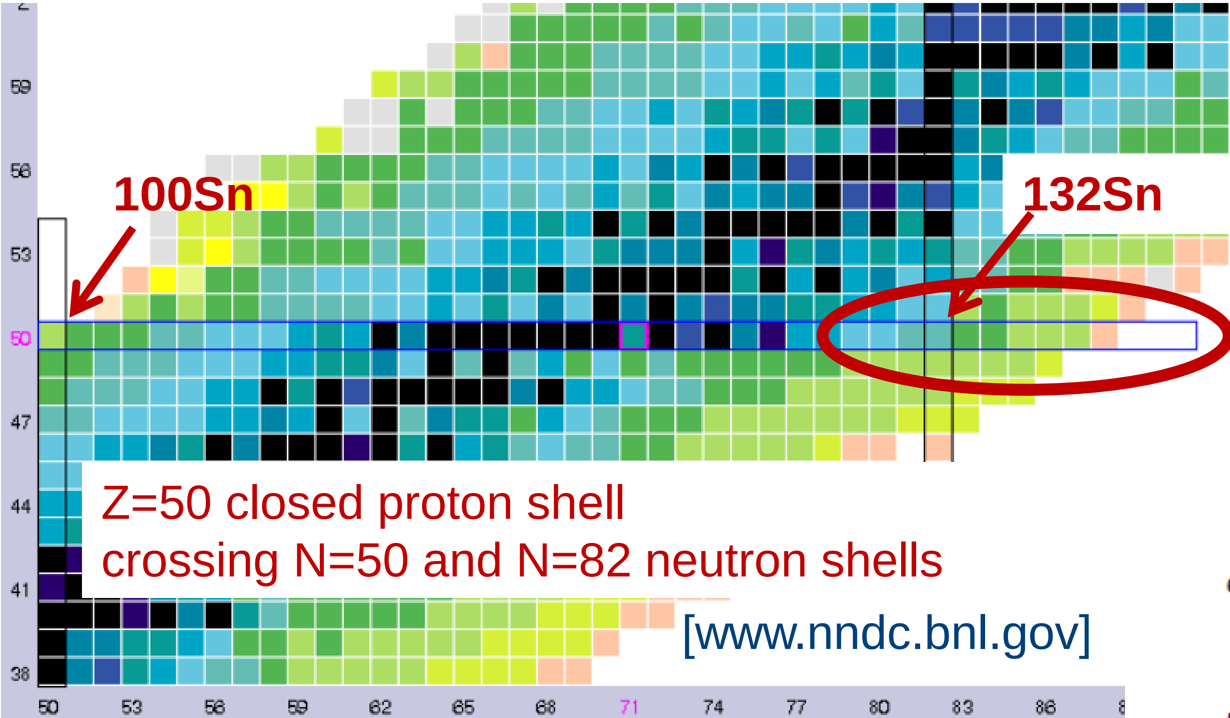

Z=50 closed proton shell
crossing N=50 and N=82 neutron shells

[www.nndc.bnl.gov]

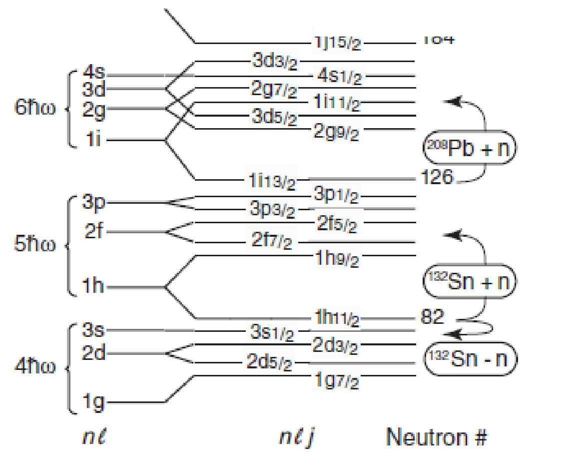

FIG. 1. Single-neutron states expected to be populated in the present one-neutron transfer study of ^{131,133}Sn and ^{209}Pb.

Shell evolution and collectivity in Tin isotopes

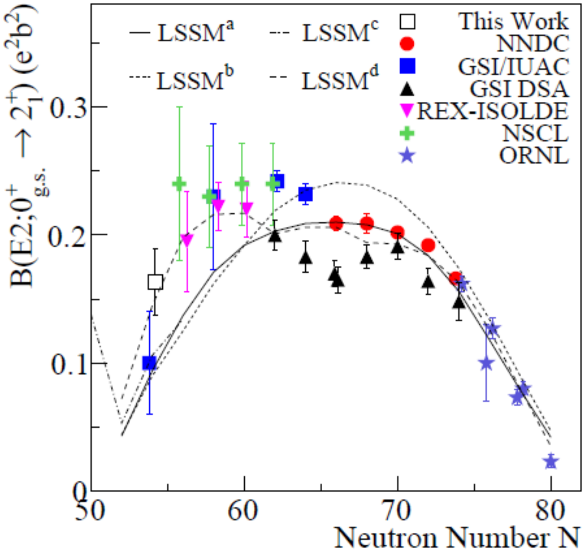

[V.M. Bader et al, PRC 88, 051301(R) (2013)]

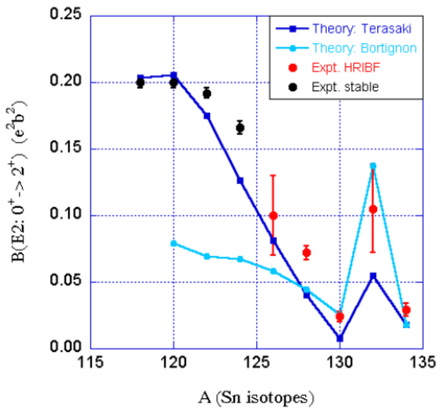

[R.L. Varner et al, EPJA 25 (2005) 391]

^{132,134}Sn Coulex @ HRIBF
9000 ions/s
150 BaF_2 (~30% eff)

^{9}Be(^{137}Sb,^{136}Sn) @ RIKEN
DALI2 (186 NaI(Tl)~22% eff)

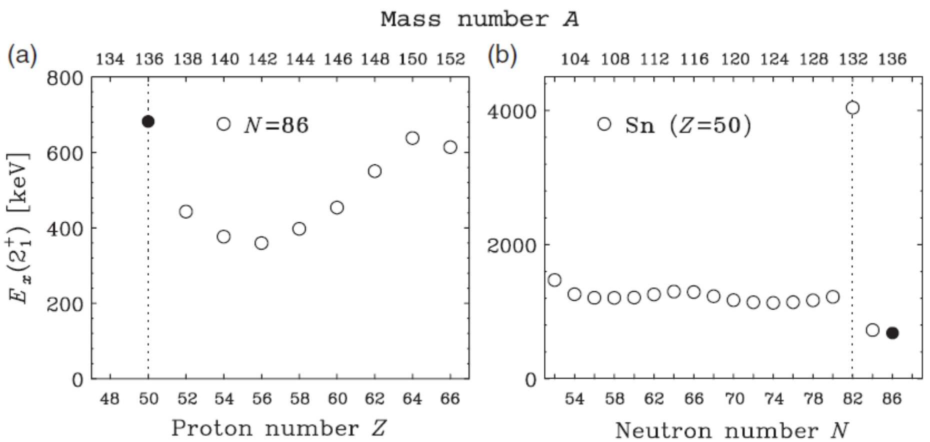

[He Wang et al, PTEP 023D02 (2014)]

Getting more details - transfer reactions

MagicTin

- **Probe single particle properties determining spectroscopic factors**
- **Extend towards more neutron-rich region (+1n)**

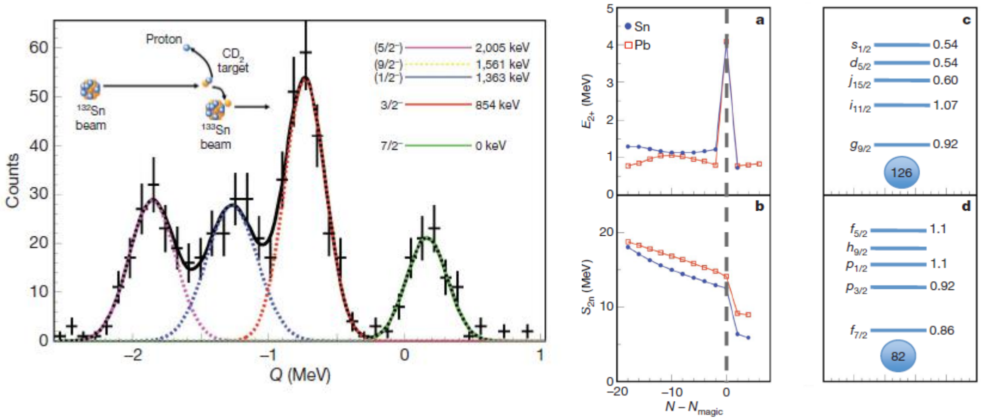

[K.L. Jones et al, Nature 465 (2010) 454]

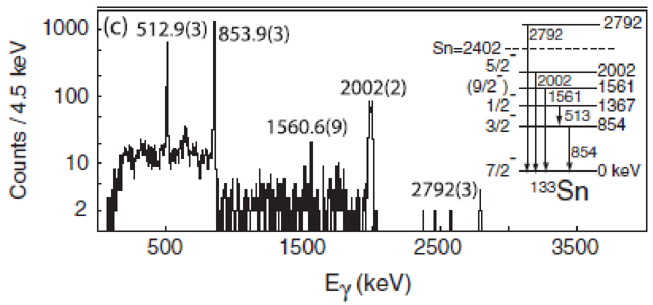

[J.M. Allmond et al, PRL 112, 172701 (2014)]

Evidences of ^{132}Sn double magicity
Resolution ~ 300 keV

High resolution spectroscopy for ^{131}Sn ^{133}Sn using (^{9}Be, ^{8}Be) transfer reactions

Beyond ^{132}Sn

Expected beam intensities @ 10 AMeV		
	SPES 1st day (5 µA p beam)	SPES full power (200 µA p beam)
^{132}Sn	7.8 10^5	3.1 10^7
^{133}Sn	7.0 10^4	2.8 10^6
^{134}Sn	1.2 10^4	4.9 10^5
^{135}Sn	1.6 10^2	6.2 10^3
^{136}Sn	-	0.9 10^2

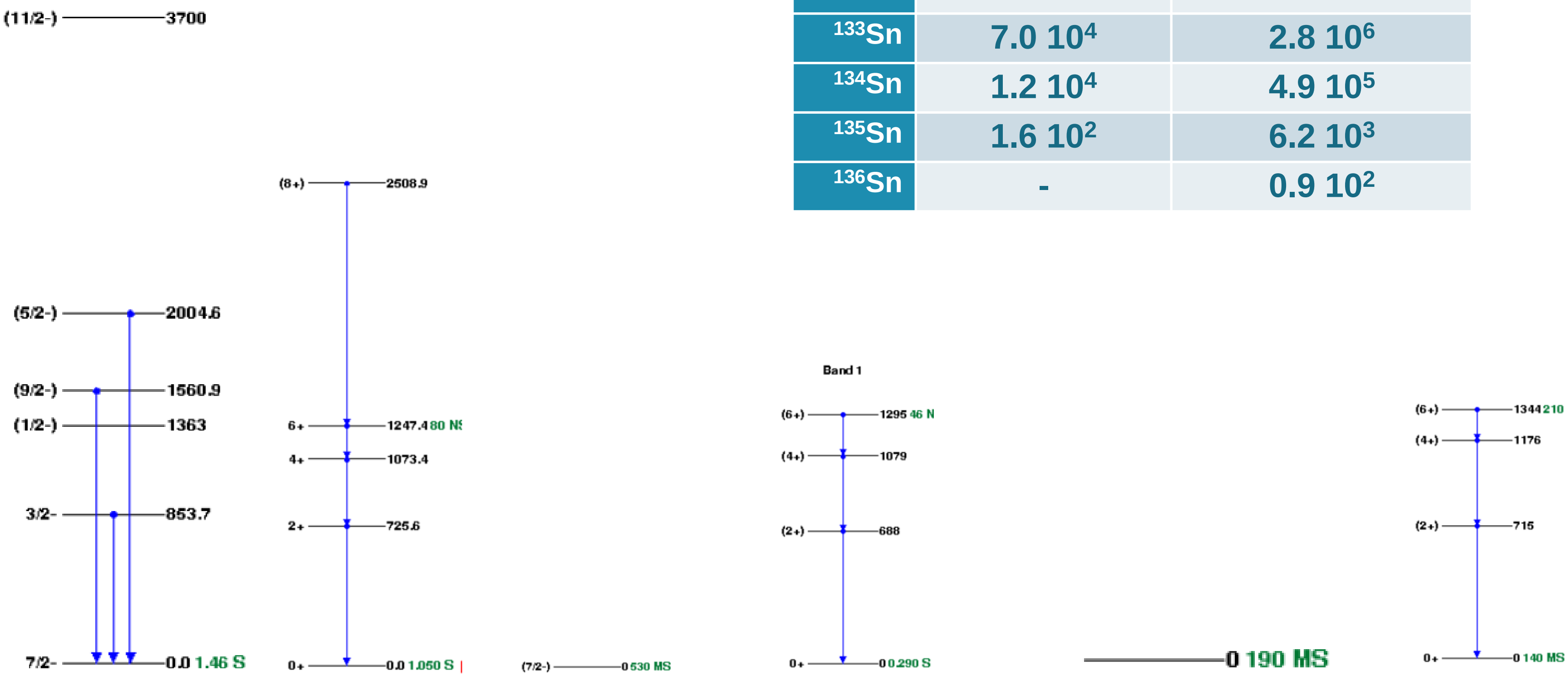

^{133}Sn — d(^{132}Sn,^{133}Sn)p, Q = 177 keV

^{134}Sn — d(^{133}Sn,^{134}Sn)p, Q_{gs} = 1.4 MeV

^{135}Sn — d(^{134}Sn,^{135}Sn)p, Q = 47 keV

^{136}Sn — d(^{135}Sn,^{136}Sn)p, Q = 1.1 MeV

^{137}Sn — d(^{136}Sn,^{137}Sn)p, Q = -264 keV

^{138}Sn — d(^{137}Sn,^{138}Sn)p, Q = 0.9 MeV

$f_{7/2}$ vs $p_{3/2}$ neutron orbitals, in Sn like in Ca?

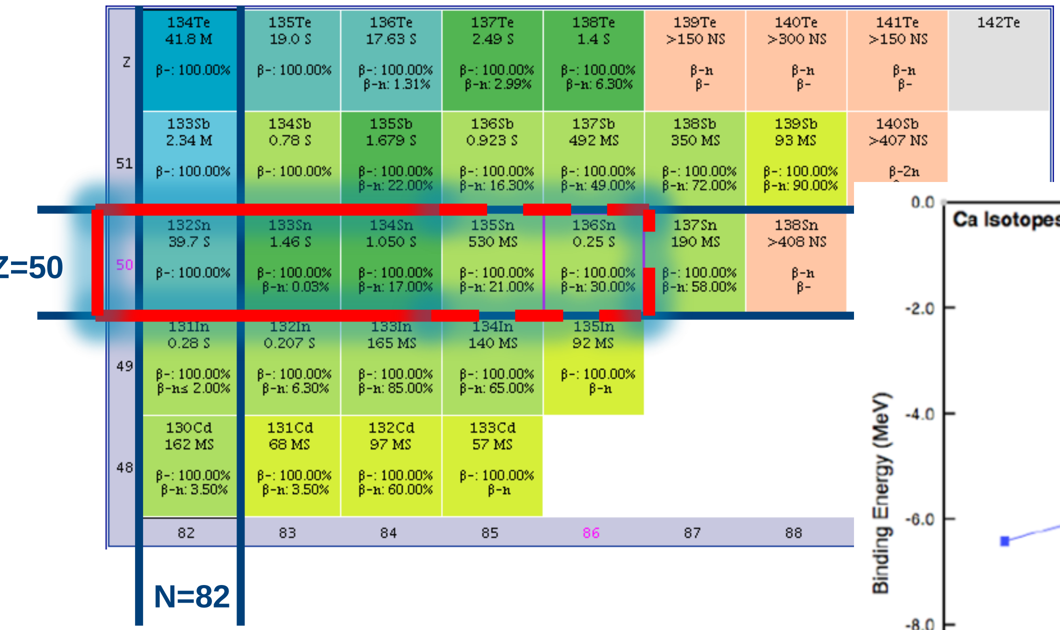

[Adapted from O. Sorlin, M.-G. Porquet, Progr Part. Nucl Phys 61 (2008) 602]

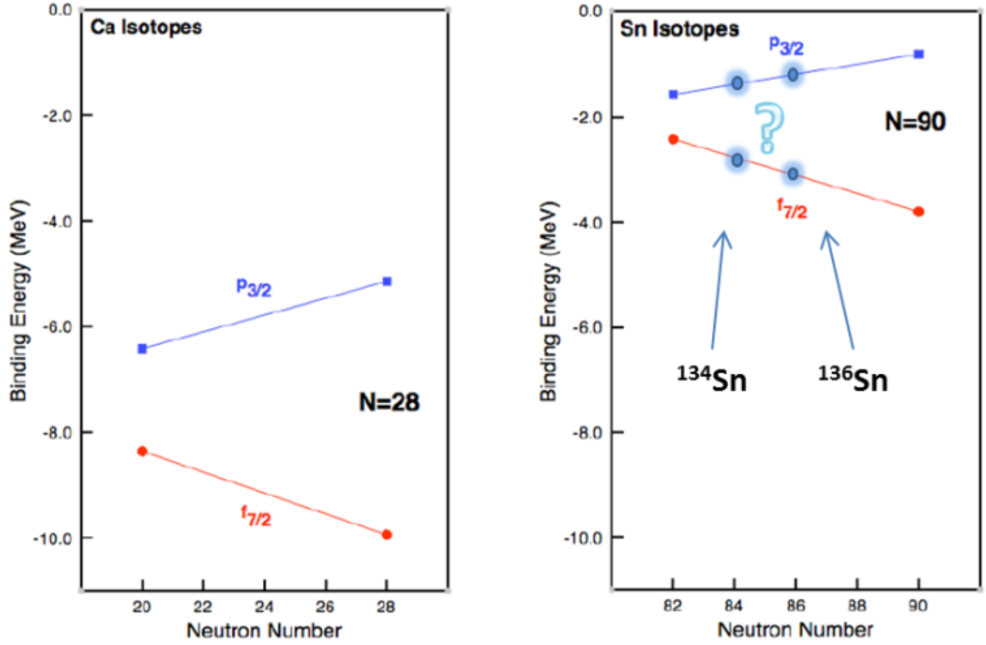

Fig.1 Analogy between f7/2 and p3/2 evolution of binding energies in the known Ca isotopes to what could be expected for the Sn isotopes approaching N=90. Figure adapted from[13].

Getting ready for RIBs: MT implementation

MagicTin*

Benchmark: $^{136}Xe(d,p)^{137}Xe$ - inv kinem

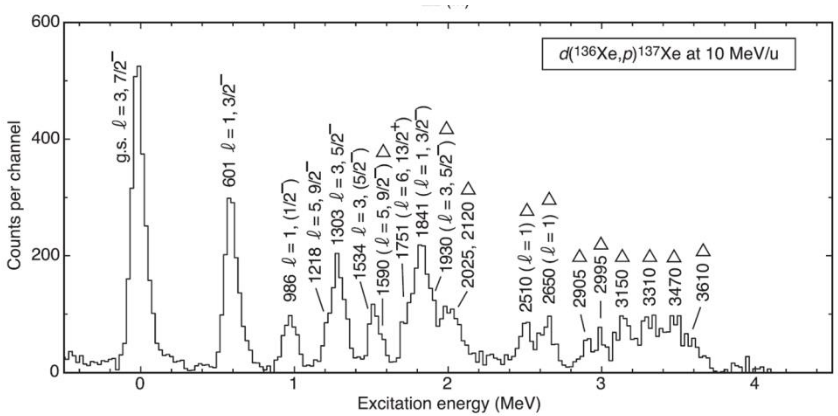

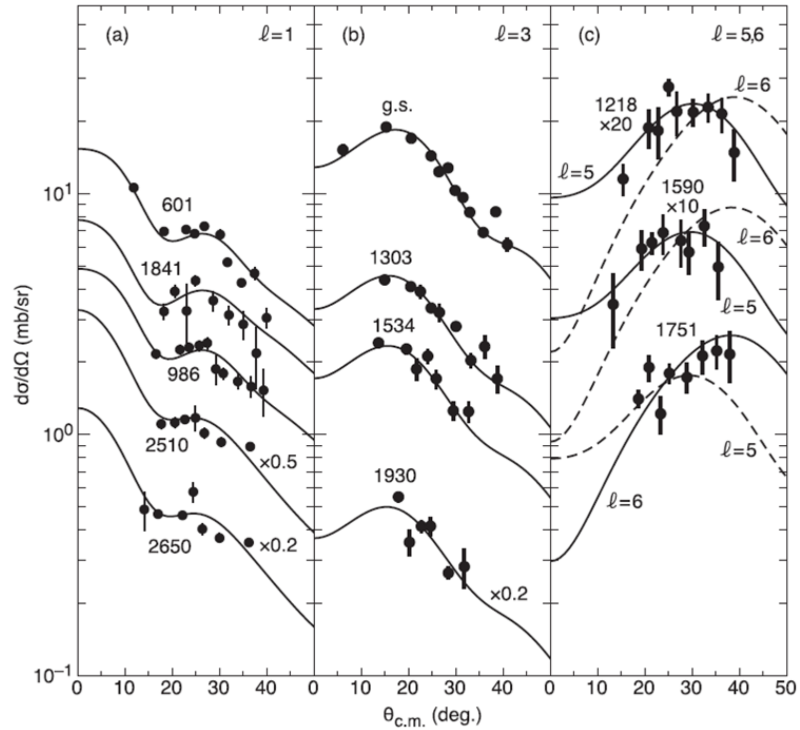

B.P. Kay et al, PRC 84 0243325 (2011)
HELIOS @ ANL

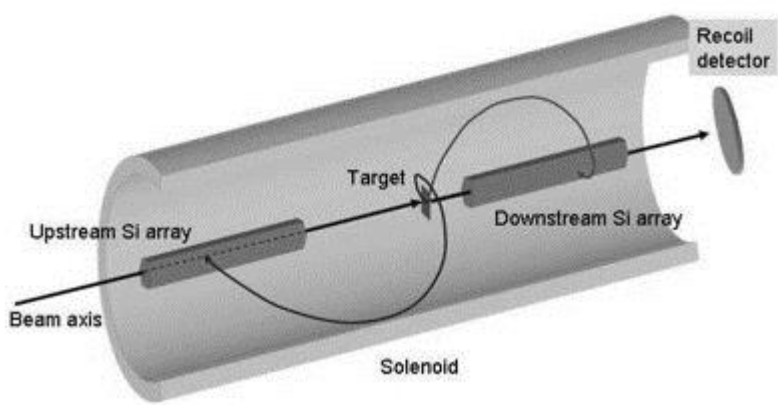

Does kinematics help?

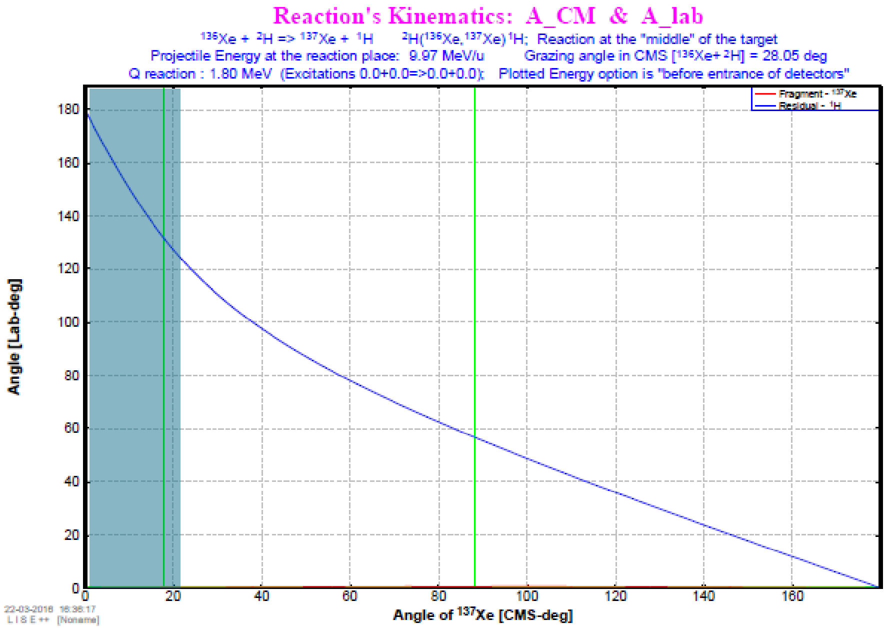

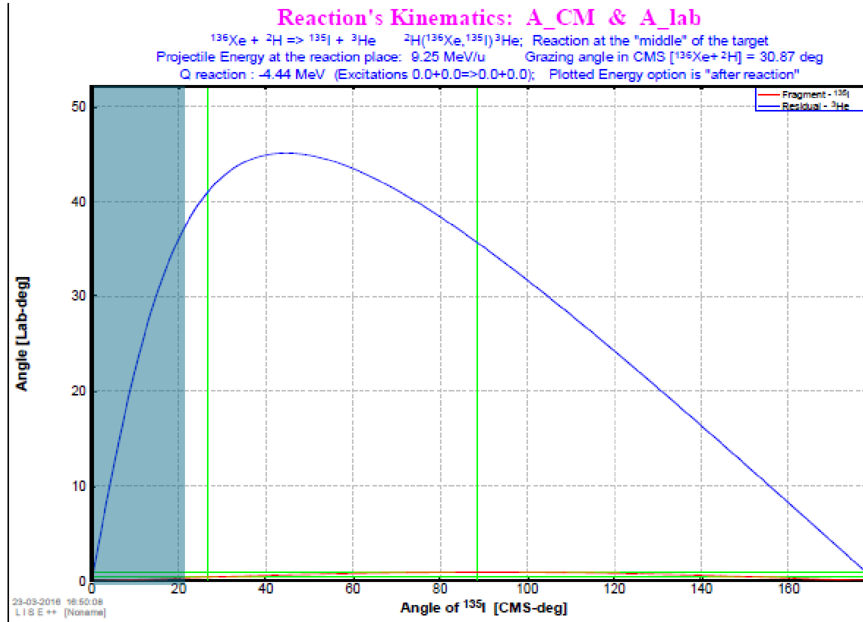

^{136}Xe(d,p)^{137}Xe - inv kinem

^{136}Xe(d,^{3}He)^{135}Ie - inv kinem

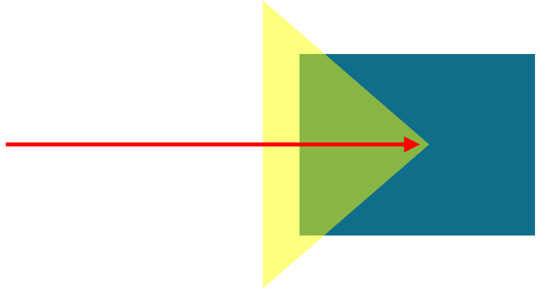

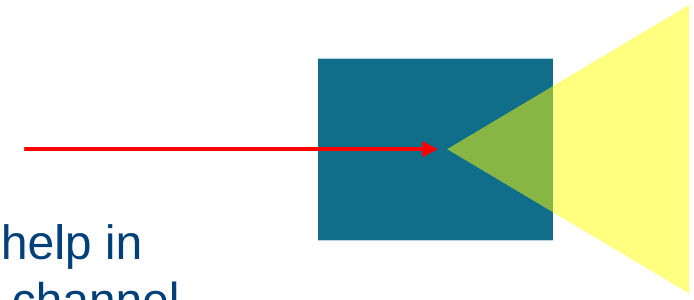

Kinematics seems to help in selecting the reaction channel

Or not?

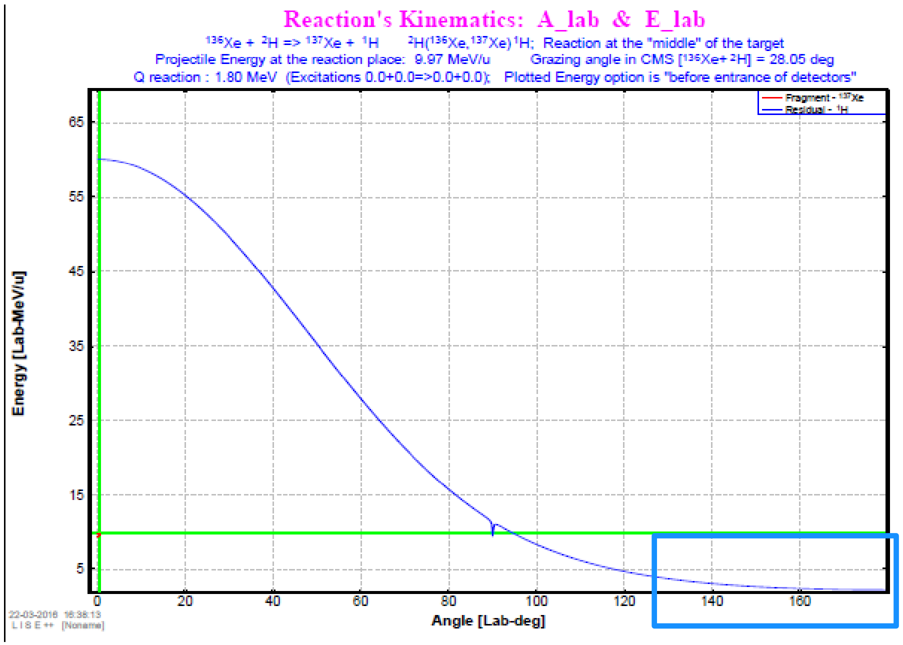

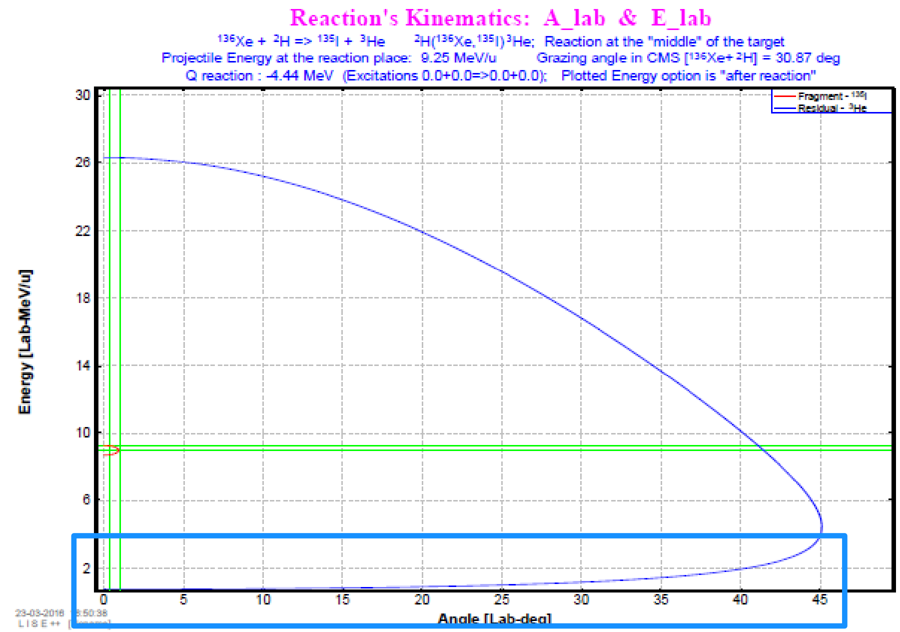

^{136}Xe(d,p)^{137}Xe - inv kinem

^{136}Xe(d,^{3}He)^{135}Ie - inv kinem

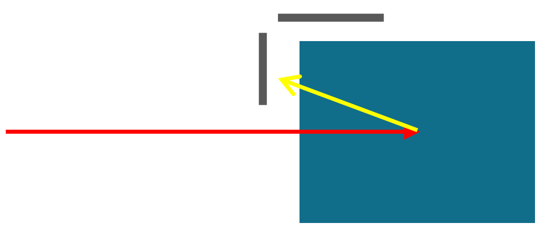

Tradeoff:
Range vs good tracking

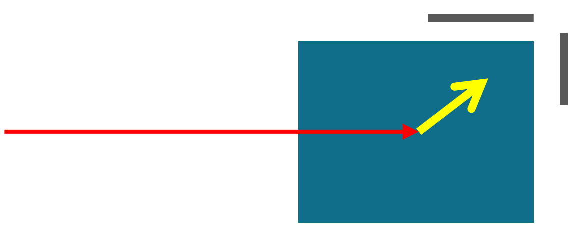

Possible setup and beams

Expected beam intensities @ 10 AMeV		
	SPES 1st day (5 µA p beam)	SPES full power (200 µA p beam)
^{132}Sn	7.8 10^5	3.1 10^7
^{133}Sn	7.0 10^4	2.8 10^6
^{134}Sn	1.2 10^4	4.9 10^5
^{135}Sn	1.6 10^2	6.2 10^3
^{136}Sn	-	0.9 10^2

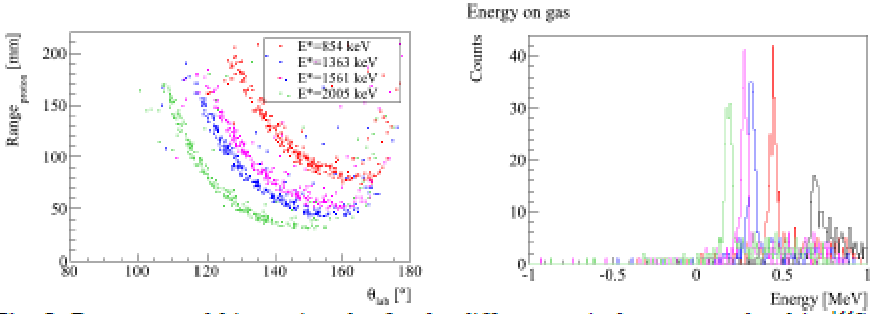

Fig. 5: Reconstructed kinematics plot for the different excited states populated in ^{133}Sn for protons stopped in the gas at a pressure of 400 mbar. Note that the majority of protons populating the ground state escape the gas and the resolution is thus slightly degraded.

Stopped in gas: ~ 110 keV FWHM res

ACTAR + Si wall

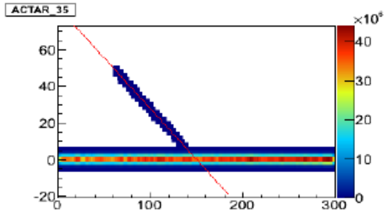

Fig. 4: Sample digitized trace for a $^{132}Sn(d,p)$ reaction with 2x2mm² sized pads. The red line corresponds to the fitted trajectory used for determining the range of the proton.

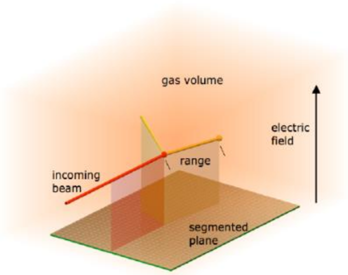

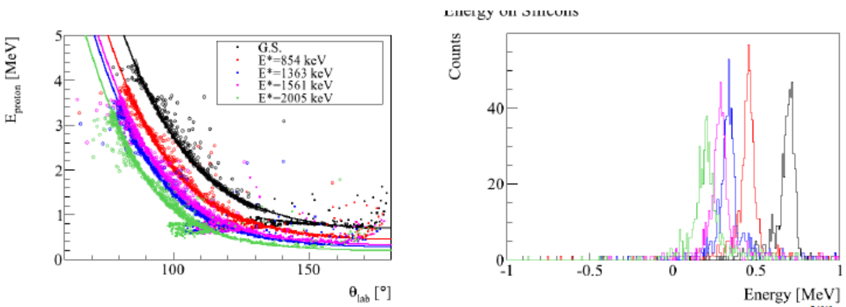

Fig. 6: Reconstructed kinematics plot for the different excited states populated in ^{133}Sn for protons stopped in the Si detectors (open circles) and stopped in the gas (closed circles).

$^{132}Sn(d,p)^{133}Sn$ @ 5 AMeV
400 mbar D_2

Gas-Si (ΔE-E): ~ 90 keV FWHM res

[D..Perez-Loureiro and G.F.Grinyer, ACTARsim Report (2013)]

Improving resolution with gamma-ray detectors

- γ-rays in PARIS-like detectors
from population of 854, 1363, 2005 keV states in ^{133}Sn

- Statistics corresponding to 2 days of beam time at 10^3 pps (total cross section 10 mb, photopeak eff 17%)

Issue: might reduce global efficiency

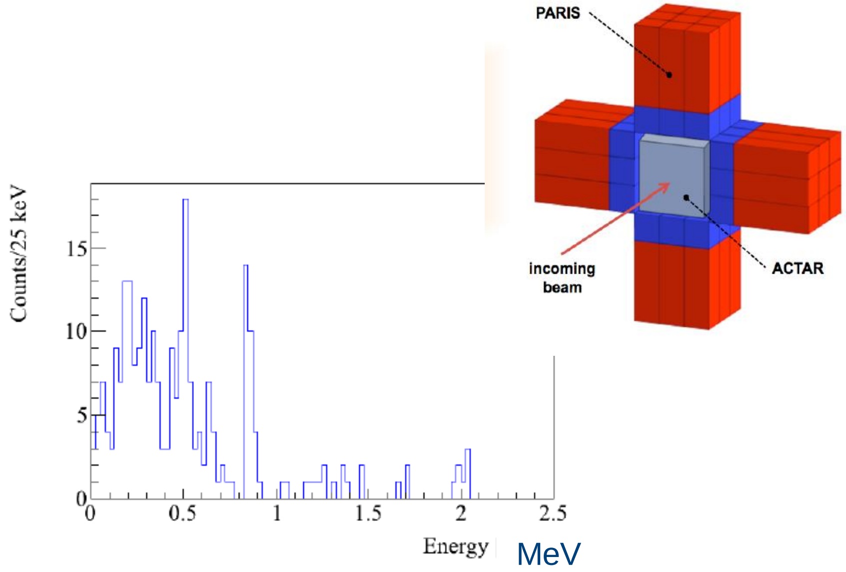

Further steps… (p,p')

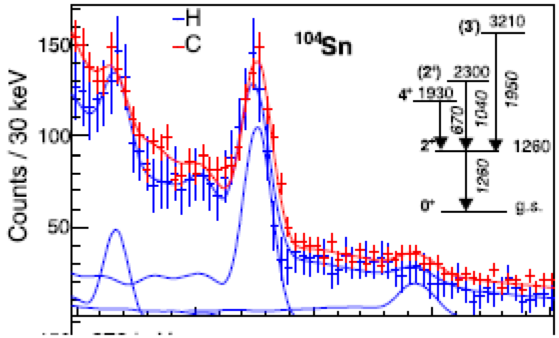

[A. Corsi et al, PLB 743 (2015) 451]

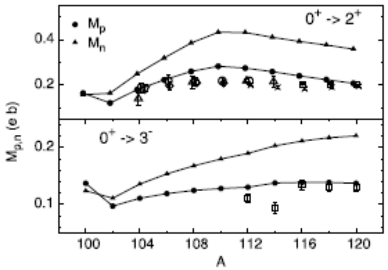

Fig. 4. M_p (•) and M_n (▲) from QRPA calculations with the Gogny D1M interaction compared to experimental M_p (∇: RIKEN [14], ○: NSCL [9,13], ×: GSI Doppler Shift Attenuation Method [34], Δ: GSI Coulomb excitation [6,10–12], ◇: ISOLDE [7,8], □: NNDC [28]). Top: 2_1^+. Bottom: 3_1^-. Experimental M_n values are taken from the literature [22].